Systematic Effects of Coal Rank and Type on the Kinetics of Coal Pyrolysis

ARTICLE *in* ENERGY & FUELS · JANUARY 2001

Impact Factor: 2.79 · DOI: 10.1021/ef000170x

5 AUTHORS, INCLUDING:

Diego Alvarez
Spanish National Research Council
37 PUBLICATIONS **1,604** CITATIONS
SEE PROFILE

Angeles Borrego
Spanish National Research Council
73 PUBLICATIONS **929** CITATIONS
SEE PROFILE

Rosa Menéndez
Spanish National Research Council
226 PUBLICATIONS **3,050** CITATIONS
SEE PROFILE

Goyo Marban
Spanish National Research Council
53 PUBLICATIONS **1,588** CITATIONS
SEE PROFILE

Systematic Effects of Coal Rank and Type on the Kinetics of Coal Pyrolysis

M. J. G. Alonso, D. Alvarez, A. G. Borrego, R. Menéndez, and G. Marbán*

Instituto Nacional del Carbón (CSIC), Apartado 73, 33080-Oviedo, Spain

In this work, the global pyrolysis kinetics of a broad range of coals was studied by means of thermogravimetric experiments (heating rate = 25 °C/min). An Arrhenius-based deconvolution model was applied to the experimental DTG curves in order to obtain reliable kinetic parameters for the different DTG peaks. The model assumes that the weight loss rate ascribed to volatile release during primary and secondary pyrolysis is a result of the parallel occurrence of three pseudo-unimolecular *n*th-order reactions (peaks *1*, *2*, and *3*). The kinetic results were expressed as a function of coal rank ($0.43 \leq R_r \leq 1.14\%$) and maceral composition in order to obtain reliable kinetic trends. By error minimization, an average apparent reaction order of 1.67 was found. The mass fractions corresponding to peaks *1*, *2*, and *3* were found to follow definite trends with rank and maceral composition. The temperature of maximum reactivity for peak *1* was almost coincident with that of the maximum overall reactivity and followed clear trends with coal rank and type. The activation energies of peaks *2* and *3* were found to be independent of coal type and clearly related to coal rank. The kinetic parameters (activation energy and preexponential factor) of the three peaks exhibited clear isokinetic effects. It is thought that the deviations of the obtained activation energies from those calculated by the isokinetic effect trends are a consequence of a narrow distribution of activation energies within each peak.

Introduction

Coal pyrolysis has been the object of numerous studies as a consequence of its paramount relevance in the processes of coal combustion and gasification. Thus, several reviews produced in the nineties[1−3] remark the influence of coal pyrolysis on softening, swelling, particle agglomeration, char reactivity, and char physical structure during combustion or gasification of coal. Additionally, tar produced during the pyrolysis stage is normally the volatile product of highest initial yield and not only controls ignition and flame stability but is also a precursor of soot, which affects the radiative heat transfer in the boiler. Pyrolysis of coal is also the basic process of cokemaking and it is a process in its own right for producing liquid and gaseous products from coal. All these points clearly justify the extensive amount of kinetic studies undergone in the past few years with the objective of obtaining reliable kinetic parameters to be used in complex models (i.e., functional group models[4−6]) that allow pyrolysis yields of various chemical species to be predicted with relative success for different heating rates, reactors, and coal types. On the other hand, these kinetic studies have also permitted us to attain a deeper knowledge on the relations existing between certain characteristics of given coals and their pyrolysis behavior, although a systematic description of coal pyrolysis is to date difficult to carry out due to the inherent heterogeneity of coal. Thus, certain attempts were performed in order to establish systematic trends of pyrolysis yields and kinetic parameters with coal variables such as rank,[7] carbon content,[8,15,16] vitrinite reflectance,[9−11,25] degree of artificial maturation,[10,12] and maceral composition[11−16,20] of coals and

* Author to whom correspondence should be addressed. Tel.: +34 985280800. Fax: +34 985297662. E-mail: greca@incar.csic.es.

(1) Saxena, S. C. Devolatilization and combustion characteristics of coal particles. *Prog. Energy Combust. Sci.* **1990**, *16*, 55−94.

(2) Solomon, P. R.; Serio, M. A.; Suuberg, E. M. Coal pyrolysis experiments. Kinetic rates and mechanisms. *Prog. Energy Combust. Sci.* **1992**, *18*, 133−220.

(3) Solomon, P. R.; Fletcher, T. H.; Pugmire, R. J. Progress in coal pyrolysis. *Fuel* **1993**, *72* (5), 587−597.

(4) Serio, M. A.; Hamblen, D. G.; Markham, J. R.; Solomon, P. R. Kinetics of volatile product evolution in coal pyrolysis: Experiment and theory. *Energy Fuels* **1987**, *1* (2), 138−152.

(5) Solomon, P. R.; Hamblen, D. G.; Carangelo, R. M.; Serio, M. A.; Despande, G. V. General model of coal devolatilization. *Energy Fuels* **1988**, *2* (4), 405−422.

(6) Solomon, P. R.; Serio, M. A.; Despande, G. V.; Kroo, E. Cross-linking reactions during coal conversion. *Energy Fuels* **1990**, *4* (1), 42−54.

(7) van Heek, K. H.; Hodek, W. Structure and pyrolysis behaviour of different coals and relevant model substances. *Fuel* **1994**, *73* (6), 886−896.

(8) Burnham, A. K.; Oh, M. S.; Crawford, R. W.; Samoun, A. M. Pyrolysis of Argonne Premium coals: activation energy distributions and related chemistry. *Energy Fuels* **1989**, *3* (1), 42−55.

(9) Delvaux, D.; Martin, H.; Leplat, P.; Paulet, J. Geochemical characterization of sedimentary organic matter by means of pyrolysis kinetic parameters. *Org. Geochem.* **1990**, *16* (1−3), 175−187.

(10) Schenk, H. J.; Horsfield, B. Using natural maturation series to evaluate the utility of parallel reaction kinetics models: an investigation of Toarcian shales and carboniferous coals, Germany. *Org. Geochem.* **1998**, *29* (1−3), 137−154.

(11) Borrego, A. G.; Marbán, G.; Alonso, M. J. G.; Álvarez, D.; Menéndez, R. Maceral effects in the determination of proximate volatiles in colas. *Energy Fuels* **2000**, *14* (1), 117−126.

(12) Carlsen, L.; Feldthus, A.; Landais, P. Solid-state pyrolyses: Part 4. Kinetic evaluation of coal pyrolyses: effects of maturation. *J. Anal. Appl. Pyrol.* **1993**, *26*, 115−125.

(13) Xie, K.-Ch.; Zhang, Y.-F.; Li, Ch-Z.; Ling, D.-Q. Pyrolysis characteristics of macerals separated from a single coal and their artificial mixture. *Fuel* **1991**, *70*, 474−479

(14) White, A.; Davies, M. R.; Jones, S. D. Reactivity and characterization of coal maceral concentrates. *Fuel* **1989**, *68*, 511−519.

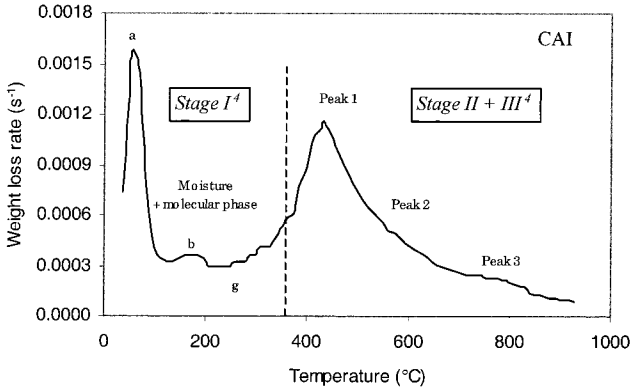

Figure 1. Typical weight loss rate variation during a nonisothermal pyrolysis experiment (sample: CAI; β = 25 °C/min).

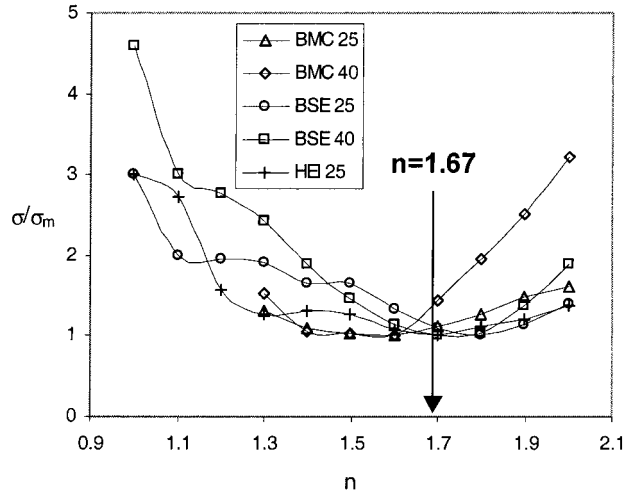

Figure 2. Normalized sum of square deviations between the experimental and calculated reactivity curves as a function of the apparent reaction order for coals BMC, BSE, and HEI (heating rates = 25 and 40 °C/min).

organic sediments. Except for the maceral composition, the rest of the variables are closely related to the maturation degree of the material. From a petrographic point of view, the combination of maturation degree and maceral composition constitutes the fingerprint of a coal, and therefore a rigorous analysis of the pyrolysis process should consider the separate effect of both variables.

A few works can be found in the literature on the simultaneous effect of maturation degree and maceral composition on global pyrolysis yields. One of the most recent studies[15] reported systematic trends in pyrolysis yields with original carbon content for maceral concentrates submitted to high heating rate experiments. In an even newer study by Borrego et al.[11] a series of equations were produced that allow the proximate volatile content of a given coal to be predicted from its maceral composition and vitrinite reflectance. On the other hand, there is surprisingly very little information on the simultaneous influence of these variables on pyrolysis kinetics. White et al.[14] carried out thermogravimetric pyrolysis of maceral concentrates of different ranks ($0.44 < R_r < 0.91\%$) and studied the DTG curves in terms of weight loss rates (reactivity) in the temperature range 350−950 °C, although no other kinetic parameters (i.e., activation energy) were reported. They found that in general all coals and their

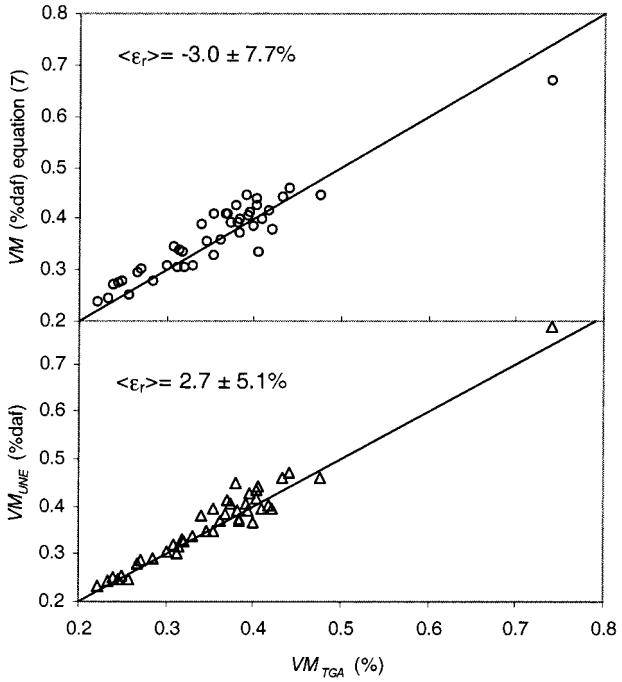

Figure 3. Comparison between the values of volatile matter estimated from the TGA experiments (VM_{TGA}) and those estimated by the UNE standard (VM_{UNE}) and by eq 7.

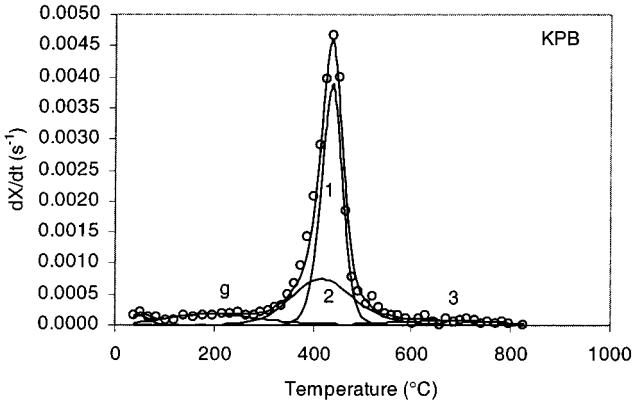

Figure 4. Temperature-reactivity profile of KPB (β = 25 °C/min) and deconvolution results.

(15) Cai, H.-Y.; Megaritis, A.; Messenböck, R.; Dix, M.; Dugwell, D. R.; Kandiyoti, R. Pyrolysis of coal maceral concentrates under pf-combustion conditions (I): changes in volatile release and char combustibility as a function of rank. *Fuel* **1998**, *77* (*12*), 1273−1282.

(16) Cai, H.-Y.; Megaritis, A.; Messenböck, R.; Vasanthakumar, L.; Dugwell, D. R.; Kandiyoti, R. Pyrolysis of coal maceral concentrates under pf-combustion conditions (II): changes in heteroatom partitioning as a function of rank. *Fuel* **1998**, *77* (12), 1283−1289.

(17) Wutti, R.; Petek, J.; Staudinger, G. Transport limitations in pyrolysing coal particles. *Fuel* **1996**, *75* (7), 843−850.

(18) Seebauer, V.; Petek, J.; Staudinger, G. Effects of particle size, heating rate and pressure on measurement of pyrolysis kinetics by thermogravimetric analysis. *Fuel* **1997**, *76* (13), 1277−1282.

(19) Lázaro, M. J.; Moliner, R.; Suelves, I. Nonisothermal versus isothermal technique to evaluate kinetic parameters of coal pyrolysis. *J. Anal. Appl. Pyrol.* **1998**, *47*, 111−125.

(20) Tsai, Ch-Y.; Scaroni, A. W. Pyrolysis and combustion of bituminous coal fractions in an entrained-flow reactor. *Energy Fuels* **1987**, *1* (3), 263−269.

(21) Chermin, H. A. G.; van Krevelen, D. W. Chemical structure and properties of coal. XVII − A mathematical model of coal pyrolysis. *Fuel* **1957**, *36*, 85−104.

(22) Carlsen, L.; Feldthus, A.; Bo, P. Solid-state pyrolyses: Part 2. Solid-state kinetics studied by pyrolysis-gas chromatography. *J. Anal. Appl. Pyrol.* **1991**, *19*, 15−27.

(23) Burnham, A. K.; Braun, R. L. Global kinetic analysis of complex materials. *Energy Fuels* **1999**, *13* (1), 1−22.

(24) Miura, K. A new and simple method to estimate f(E) and k_o(E) in the distributed activation energy model from three sets of experimental data. *Energy Fuels* **1995**, *9* (2), 302−307.

(25) Burnham, A. K.; Sweeney, J. J. A chemical kinetic model of vitrinite maturation and reflectance. *Geochim. Cosmochim. Acta* **1989**, *53*, 2649−2657

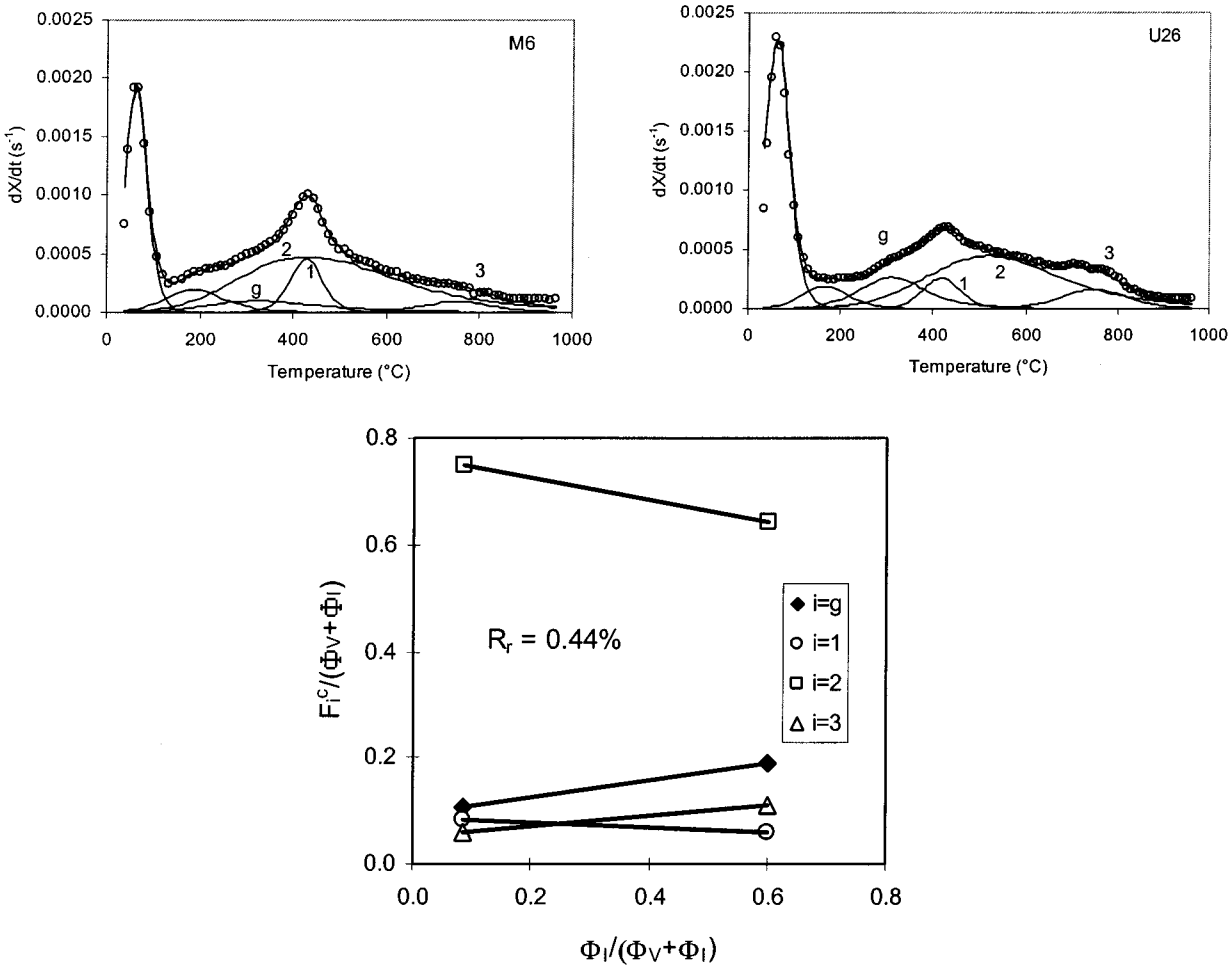

Figure 5. Reactivity profiles and deconvolution results of M6 and U26 (β = 25 °C/min), used for estimating α_{iV} and α_{iI} at R_r = 0.44% by means of the $F_i^c/(\Phi_V + \Phi_I)$ regression plot.

macerals, when heated either in nitrogen or in hydrogen, showed single peaks at about 500−520 °C (heating rate: β = 20 °C/min). Up to 600 °C, the reactivity order was liptinite > vitrinite > inertinite. Above 600 °C, the order of reactivity was generally vitrinite > inertinite > liptinite. These authors also carried out functional group analysis by infrared spectroscopy of fresh and partially devolatilized maceral concentrates. The fresh liptinite concentrates were found to be rich in aliphatic hydrogen, whereas inertinites contained a higher proportion of aromatic hydrogen, being the vitrinites in an intermediate position. By comparison of the fresh and partially devolatilized samples, aliphatic hydrogen was shown to be volatile in the range 350−650 °C, temperatures at which aromatic hydrogen was found to be rather stable. The volatile yield of liptinites was found to be independent of atmosphere (N_2 or H_2) and pressure, suggesting that the aliphatic hydrogen loss is essentially due to a thermal degradation process. Other works on the effect of maturation and maceral composition on pyrolysis kinetics are focused on sedimentary organic matter with the goal of obtaining kinetic parameters for kerogen degradation to be used either in predictive models of hydrocarbon generation in sedimentary basins[9] or for organic matter classification.[10] Thus, Delvaux et al.[10] used a single *n*th-order overall reaction scheme to construct kinetic diagrams in which several composition indexes (hydrogen, oxygen, and paraffin−aromatic contents) of different types of kerogen of varying rank were represented as a function of the obtained activation energies and the reaction orders. They found that activation energy (E) alone was insufficient for the classification of organic matter, necessitating the use of a second parameter. Thus, the ratio of activation energy to reaction order (E/n) was found to have well-defined ranges and could be used for the determination of resins + asphaltenes type in the rock samples.

All these works are, however, rather specific and either do not use the common Arrhenius parameters in the search of systematic trends[14] or cover a small spectrum of materials.[10] In this work the global pyrolysis kinetics of a broad range of coals is studied with the goal of obtaining reliable and systematic trends in the kinetic parameters with maturation degree and maceral composition.

Experimental Section

Thirty coals, five hand-picked coals and six density-separated fractions of different provenance, geological age, and maceral composition, covering a wide range of maceral occurrences and ranks (vitrinite random reflectance from 0.43 to 1.14%), were analyzed for proximate, maceral, and vitrinite random reflectance standard analyses (Table 1). Proximate volatiles were obtained following the standard UNE 32-019-84 and the values were corrected for the CO_2 evolved from carbonates calcinations as described in ISO-168. The data were expressed in dry, ash-free basis, for which ash contents were obtained following the standard ISO-1171/1981. Low-ash coals (<15%) were used in order to minimize the errors arising from the mass losses of mineral matter upon heating. Thus, the

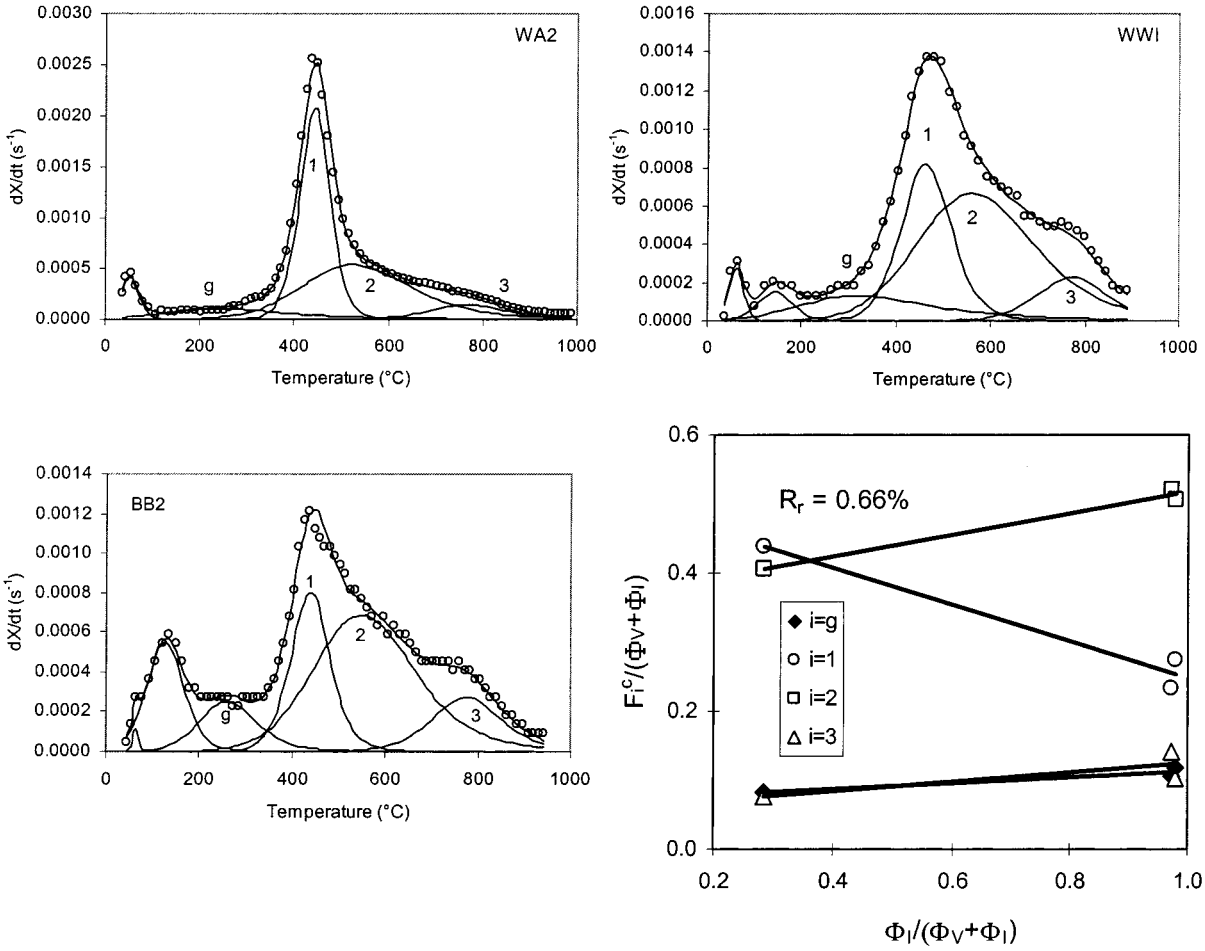

Figure 6. Reactivity profiles and deconvolution results of WA2, WWI, and BB2 (β = 25 °C/min), used for estimating α_{iV} and α_{iI} at R_r = 0.66% by means of the $F_i^c/(\Phi_V + \Phi_I)$ regression plot.

coals with an initial mineral matter content higher than 15% were floated with dense liquids, and the floated fractions were used.

Petrographic analyses were carried out by combined maceral/reflectance analysis using a Leitz Combi photomicroscope, non polarized light, and oil immersion objective of 50× magnification. Random reflectance readings were taken on 500 macerals selected by point counting, and the corresponding maceral was annotated. For rank determination, the readings taken on telocollinite were averaged.

An oil shale from Puertollano (Spain; type I kerogen; 100% liptinite) was used for obtaining the DTG profile of a pure liptinite sample. The proximate and petrographic analyses of this sample are indicated in Table 1.

Prior to the pyrolysis experiments, the samples were ground and sieved to the size fraction 36−75 μm. The pyrolysis experiments were conducted in a Perkin-Elmer TGA7 thermogravimetric analyzer (TGA). Coal samples with a weight in the range 10−15 mg (differential conditions) were distributed on the bottom of the platinum crucible of the TGA. N_2 was passed through the reaction chamber at ambient temperature during 45 min to sweep away any oxygen trace. The samples were then heated to 900 °C (1000 °C in a few occasions) at a heating rate of 25 °C/min (40 °C/min in specific experiments), and maintained at that temperature for 1 h before switching the gas to air. By this procedure, the organic matter of the pyrolyzed sample was burnt out, so that the ash content of the sample could be estimated. After stabilization of its weight, the sample was cooled to ambient temperature and the experiment was ended. There were not limitations in mass and/or heat transfer derived from the used experimental setup and conditions (heating rate, particle size, and temperature).[17,18]

Kinetic Modeling Based on Overall Weight Losses. Global pyrolysis kinetics of coal has been studied during the last years via a variety of experimental procedures and mathematical schemes. Nowadays it is recognized that nonisothermal techniques are more powerful than isothermal techniques to evaluate kinetic parameters of coal pyrolysis.[19] The former can be readily utilized in thermogravimetric analyzers that have an important advantage over other apparatuses, as is the accurate measurement of the sample temperature[2]. DTG plots of nonisothermal pyrolysis experiments carried out in a thermogravimetric analyzer at a low heating rate (1−50 °C/min) present a typical profile similar to that shown in Figure 1 (heating rate = 25 °C/min). As indicated in the figure, adsorbed moisture is first released, with a maximum weight loss rate in the range 40−100 °C (peak *a* on the left-hand side of the dashed line). In some cases, an adjacent peak with a maximum weight loss rate at around 150 °C takes place (peak *b* on the left-hand side of the dashed line). This peak might be ascribed to release of either crystal water from the mineral matter of the coal or chemically bonded moisture.[33] Simultaneously, the vaporization and transport of noncovalently bonded "guest" molecules[2] (molecular phase) starts to take place. This zone (zone *g* to the left-hand side of the dashed line in Figure 1) corresponds to stage I of the model proposed by Serio et al.,[4] which is an extension of a model originally proposed by Chermin and van Krevelen.[21] These molecules trapped in the coal matrix and desorbed at relatively low temperature (<350 °C) are not considered primary pyrolysis products and in some works are eliminated prior to performing the pyrolysis experiments via solvent-extraction or ther-

(26) Misra, M. K.; Essenhigh, R. H. Release of volatiles from pyrolyzing coal particles: Relative roles of kinetics, heat transfer, and diffusion. *Energy Fuels* **1988**, *2* (4), 371−385.

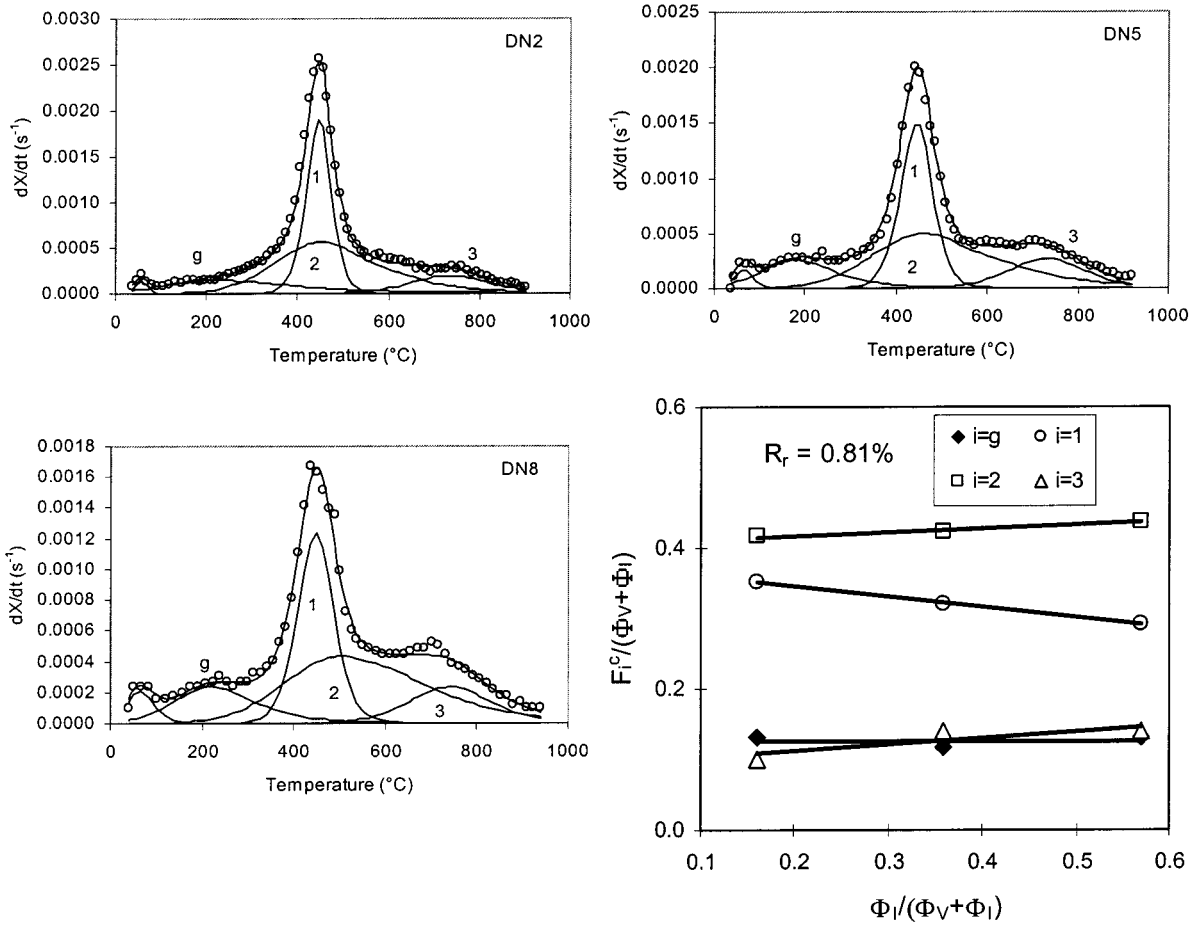

Figure 7. Reactivity profiles and deconvolution results of DN2, DN5, and DN8 (β = 25 °C/min), used for estimating α_{iV} and α_{iI} at R_r = 0.0.81% by means of the $F_i^c/(\Phi_V + \Phi_I)$ regression plot.

movaporization.[22] Finally, stages II (primary pyrolysis) and III (secondary pyrolysis) of the model by Serio et al.,[4] which comprise the processes of release of tar (stage II), primary gases (II), and secondary gases (III), and the final formation of char, produce a profile in the DTG curve as that shown in Figure 1 (right-hand side of the dashed line). This profile seems to be formed by two peaks that are clearly distinguishable (peaks *1* and *3*) and a third peak (peak *2*), which is inferred from the need of connecting peaks *1* and *3*. This behavior is consistent with the description of coal pyrolysis reported by van Heek and Hodek.[7] These authors observe three reaction peaks during primary and secondary pyrolysis. The degradation of the macromolecular structure proceeds in two steps: between 400 and 450 °C and between 500 and 550 °C. In both reactions, tar and gases are formed. The third reaction peak appears at ~700 °C, where the breakdown of the coal structure is completed and char has been formed. In this char there are some oxygen-containing structures which are decomposed with the formation of carbon monoxide. Methane is also released in this stage.

The most commonly used reactivity equation for analyzing global kinetics of coal pyrolysis is that based on a pseudo-unimolecular *n*th-order reaction:[23]

$$\frac{dX}{dt} = k(1 - X)^n \qquad (1)$$

where X is the mass fraction of released volatiles at a time t and k is the overall reaction rate constant. It is further assumed that the temperature dependence of the rate constant, k, is given by the empirical Arrhenius equation

$$k = A \times e^{-E/RT} \qquad (2)$$

where A is the preexponential or frequency factor, E is the activation energy, R is the universal gas constant, and T is the absolute temperature. However, the asymmetric profile of the pyrolysis DTG plots of many coals (i.e., Figure 1) makes the use of eq 1 impractical in the search of a single triplet of values (A, E, n) valid for a broad temperature range. Instead, more or less refined distributed activation energy (DAE) models[23,24,28−30] are commonly applied. These models assume that the distribution of reactivity caused by the reaction complexity can be represented by a set of independent, parallel reactions, each with their own values of A_i and E_i (a first order is assumed). A simplified DAE model considers a fixed frequency factor, which is common to all the activation energies of the distribution.[30] This simplification is, however, criticized by some authors[24,27] who consider that the commonly found relationship between frequency factor and activation energy, known as the isokinetic effect,[26,27] must be included in the calculation procedure. Other serious criticism[24,27] to the common DAE models is the use of continuous distribution curves (i.e., Gaussian) for the activation energy, which are normally characterized by an average activation energy and a standard deviation of energies (σ). Instead, a numerical recipe for the search of discrete distribution functions is preferred.[24,27]

In this work we propose to combine the pseudo-unimolecular *n*th-order reaction scheme with a discrete DAE model, which is a refinement of a previously reported model.[31] The main assumption of this model is that, for any given coal, the overall weight loss rate ascribed to volatile release during stages II and III of the model by Serio et al.[4] is a result of the parallel occurrence of three pseudo-unimolecular *n*th-order reactions. This implies that the asymmetry observed to the right-hand side of the dashed line in Figure 1 is produced by the overlapping of three distinct *n*th order peaks (peaks *1*, *2*, and *3*), as was already suggested. As a whole, the nonisothermal

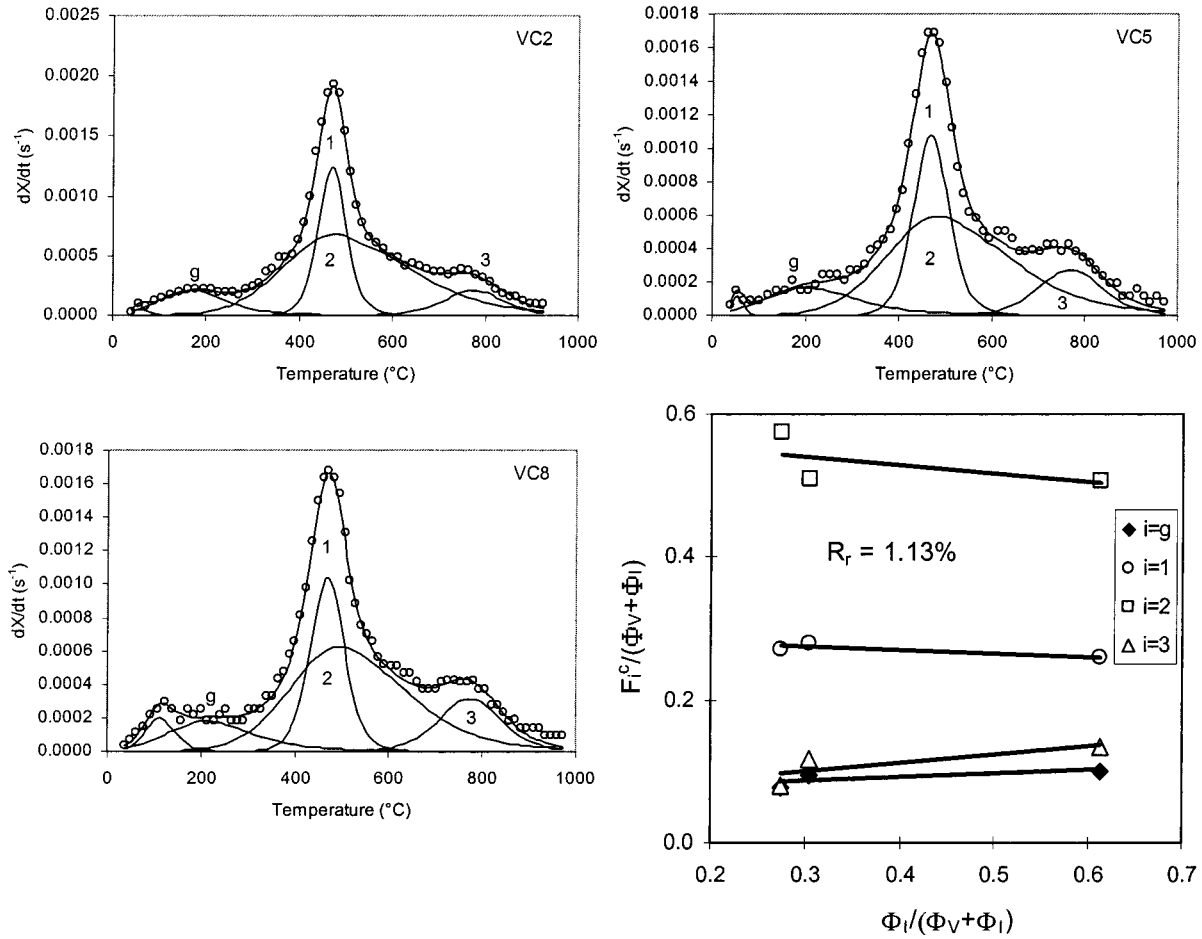

Figure 8. Reactivity profiles and deconvolution results of VC2, VC5, and VC8 (β = 25 °C/min), used for estimating α_{iV} and α_{iI} at R_r = 1.13% by means of the $F_i^c/(\Phi_V + \Phi_I)$ regression plot.

reactivity curve can be constructed by the lumped contribution of moisture release, trapped gases desorption ("molecular phase" in the model by Serio et al.[4]) and peaks *1*, *2*, and *3*. According to this, the following reactivity equation can be used for the entire temperature range (i.e., 30−900 °C):

$$\frac{dX}{dt} = f_a \frac{dX_a}{dt} + f_b \frac{dX_b}{dt} + f_g \frac{dX_g}{dt} + \sum_{j=1}^{3} f_j \frac{dX_j}{dt} = f_a k_a (1 - X_a)^n + f_b k_b (1 - X_b)^n + f_g k_g (1 - X_g)^n + \sum_{j=1}^{3} f_j k_j (1 - X_j)^n \quad (3)$$

In this equation, subscripts *a*, *b*, *g*, *1*, *2*, and *3* refer to the different DTG peaks during the nonisothermal heating (speculative assignation: *a*,*b*: water; *g*: trapped gases; *1*,*2*,*3*: peaks *1*, *2*, and *3* of primary and secondary pyrolysis), X_i (i= *a*, *b*, *g*, *1*, *2*, and *3*) is the conversion degree of process i at a time t, f_i (i= *a*, *b*, *g*, *1*, *2*, and *3*) is the mass fraction of release i on total mass release basis, k_i (i= *a*, *b*, *g*, *1*, *2*, and *3*) is the kinetic rate constant of process i, and n is the reaction order. Peaks *a*, *b*, *g*, *1*, *2*, and *3* are representative of the different mass losses during heating. However, the exact correspondence between released products and mass losses can only be done if product analysis is performed on line. In this work product analysis was not possible and therefore the peak assignations, as described above, are based on literature. Peaks *a*, *g*, *1*, *2*, and *3* were needed in order to construct the pyrolysis DTG curve of all samples. Peak *b* was absent in 29 out of the 42 samples indicated in Table 1. It must be said that the only reason to include peaks *a* and *b* in the deconvolution procedure is to avoid the error committed through eventual overlapping of these peaks with peaks *g*, *1*, *2*, and *3*.

The kinetic rate constant of the different processes can be expressed in terms of the known Arrhenius equation:

$$k^i = A_i \exp\left(-\frac{E_i}{RT}\right) \quad i = a, b, g, 1, 2, 3 \quad (4)$$

where A_i and E_i are the preexponential factor and the activation energy of process i, respectively. Either analytical approximations or numerical methods can be used to integrate eq 3. In this work, the most common approximated solutions were compared to the explicit one-step method.[23] The latter resulted to be more accurate than the approximated solutions in the zone of higher temperatures, and therefore was selected for the integration of eq 3. The numerical procedure for n=1 and n≠1 is based on eqs 5 and 6, respectively:

$$X_{i,a} = 1 - \exp\left[\ln(1 - X_{i,a-1}) - \int_{t_{a-1}}^{t_a} A_i \exp\left(-\frac{E_i}{RT}\right) dt\right] \quad i = a, b, g, 1, 2, 3\ (n = 1) \quad (5)$$

$$X_{i,a} = 1 - \exp\left[\ln(1 - X_{i,a-1})^{1-n} - (1 - n) \int_{t_{a-1}}^{t_a} A_i \times \exp\left(-\frac{E_i}{RT}\right) dt\right]^{1/1-n} \quad i = a, b, g, 1, 2, 3\ (n \neq 1) \quad (6)$$

where $X_{i,a}$ and $X_{i,a-1}$ represent the conversion degrees of process i at times t_a and t_{a-1}, respectively. The kinetic integral in eqs 5 and 6 was solved by the trapezoidal-rule method. A computer program running in a personal computer was designed in order to derive parameters f_i, A_i, and E_i in eq 3 from the numerical fitting of the experimental reactivities (dX/dt) in the temperature range 30−900 °C, via a visual collocation method. This method permits the user to have a complete

Table 1. Proximate Volatiles and Petrographic Analyses of the Used Samples[a] (the peak fractions obtained from the fitting of the DTG curves (β = 25 °C/min) are also indicated)

code	country	VM_{UNE} (daf)	R_r (%)	X_V vitrinite	X_L liptinite	X_I inertinite	F_1	F_2	F_3	F_g
					Coals					
FG2	CA	0.44	0.43	0.79	0.02	0.19	0.11	0.76	0.05	0.08
FG3	CA	0.45	0.46	0.79	0.01	0.20	0.17	0.67	0.07	0.09
CAI	BR	0.41	0.47	0.69	0.03	0.28	0.15	0.68	0.06	0.11
CAS	BR	0.40	0.48	0.58	0.09	0.33	0.20	0.61	0.07	0.13
LEA	BR	0.42	0.48	0.59	0.12	0.29	0.26	0.57	0.07	0.11
FG1	CA	0.41	0.49	0.61	0.03	0.36	0.17	0.64	0.07	0.12
INS	IN	0.46	0.55	0.92	0.04	0.04	0.39	0.50	0.05	0.06
VDR	CA	0.39	0.56	0.69	0.03	0.29	0.29	0.55	0.06	0.10
GED	UK	0.41	0.58	0.74	0.15	0.11	0.38	0.48	0.05	0.09
DRA	AU	0.39	0.59	0.50	0.09	0.41	0.37	0.46	0.07	0.10
COS	CO	0.43	0.60	0.84	0.02	0.13	0.42	0.43	0.06	0.09
CER	CO	0.39	0.61	0.82	0.01	0.17	0.41	0.44	0.06	0.08
PT2	SP	0.38	0.62	0.70	0.04	0.26	0.38	0.46	0.07	0.09
BMC	NZ	0.46	0.64	0.86	0.12	0.02	0.51	0.36	0.05	0.08
PT3	SP	0.38	0.68	0.66	0.13	0.21	0.49	0.37	0.06	0.08
SA1	SA	0.34	0.68	0.27	0.05	0.68	0.37	0.45	0.09	0.09
SA2	SA	0.31	0.68	0.31	0.03	0.66	0.36	0.43	0.11	0.09
LEM	AU	0.37	0.71	0.66	0.05	0.29	0.43	0.41	0.08	0.09
CRO	SA	0.30	0.71	0.25	0.06	0.68	0.38	0.43	0.08	0.11
KEL	UK	0.40	0.73	0.66	0.17	0.17	0.48	0.37	0.07	0.09
CAN	SP	0.39	0.74	0.90	0.05	0.05	0.45	0.40	0.07	0.09
BEN	UK	0.37	0.76	0.82	0.08	0.10	0.43	0.41	0.06	0.10
PHA	CA	0.37	0.84	0.80	0.10	0.10	0.45	0.45	0.06	0.04
CRB	CA	0.29	0.97	0.61	0.01	0.38	0.36	0.52	0.08	0.04
NOR	UK	0.32	0.98	0.73	0.10	0.17	0.39	0.46	0.06	0.08
BSE	NZ	0.32	1.03	0.96	0.04	0.00	0.33	0.52	0.05	0.09
SBA	SP	0.33	1.04	0.93	0.03	0.04	0.32	0.52	0.07	0.09
FM3	CA	0.29	1.05	0.55	0.00	0.45	0.32	0.51	0.08	0.09
FM1	CA	0.26	1.07	0.56	0.00	0.44	0.31	0.51	0.10	0.08
HEI	GE	0.28	1.14	0.78	0.05	0.18	0.32	0.54	0.07	0.08
					Hand-Picked Coals					
M6	AU	0.47	0.44	0.79	0.08	0.13	0.14	0.70	0.06	0.10
U26	AU	0.44	0.44	0.26	0.04	0.70	0.10	0.61	0.10	0.18
WA2	AU	0.37	0.66	0.57	0.04	0.39	0.45	0.40	0.07	0.08
BB2	AU	0.25	0.66	0.02	0.01	0.97	0.24	0.51	0.14	0.10
WWI	AU	0.24	0.66	0.01	0.00	0.99	0.27	0.51	0.10	0.12
					Density-Separated Fractions					
DN2	SA	0.35	0.81	0.74	0.03	0.24	0.36	0.41	0.10	0.13
DN5	SA	0.35	0.81	0.48	0.07	0.45	0.35	0.41	0.13	0.11
DN8	SA	0.33	0.81	0.28	0.08	0.64	0.34	0.42	0.12	0.12
VC2	SA	0.25	1.13	0.63	0.01	0.37	0.27	0.57	0.08	0.08
VC5	SA	0.25	1.13	0.58	0.03	0.39	0.29	0.50	0.11	0.09
VC8	SA	0.23	1.13	0.28	0.02	0.70	0.27	0.50	0.13	0.10
					Oil Shale					
KPB	SP	0.78	0.45	0.00	1.00	0.00	0.57	0.30	0.04	0.08

[a] VM_{UNE} = volatile matter fraction calculated following the standard UNE 32-019-84, R_r = random reflectance, X_V, X_L, X_I = volume fractions of vitrinite, liptinite, and inertinite (mineral matter-free), daf = dry ash-free, F_i = mass fraction of DTG peak *i*.

control over the fitting procedure. The value of *n* was obtained by minimization of the sum of square deviations of overall reactivity for an incremental variation of *n* between 1 and 2.

Results and Discussion

Apparent Reaction Order. The apparent reaction order *n* included in eq 3 should not be understood as being related to a true chemical process. Instead it seems to depend on the distribution of kinetic parameters within each peak.[23] This fact can be visualized in the Appendix, for the combination of three model peaks of order 1. The overlapping peaks, which are the result of the deconvolution of the overall reactivity curve, have a quite symmetric profile, and therefore the expected distribution of kinetic parameters in each peak can be assumed to be narrow. This is the reason to assume the same apparent reaction order for all the peaks in eq 3. Additionally, this assumption will allow the kinetic parameters obtained for the different peaks to be compared, a task which would not otherwise be possible.[9]

The value of *n* was obtained from the reactivity curves of coals BMC (heating rate: 25 and 40 °C/min), BSE (25 and 40 °C/min), and HEI (25 °C/min). The sum of square deviations (σ) between the experimental reactivities and those estimated by eq 3 during the fitting procedure were calculated for different values of *n* (between 1 and 2) and normalized with respect to the minimum σ obtained (σ_m). The results are shown in Figure 2. The presence of a minimum in the deviation curves for values of the apparent reaction order between 1.5 and 1.9 is clearly observed. By averaging these values, an average apparent reaction order of 1.67 was obtained for all the samples. Therefore this value was used for fitting all the reactivity curves to eq 3.

Relation of DTG Peak Fractions with Maceral Composition and Rank. To relate the different peak fractions obtained from the deconvolution of the reactivity curves to the maceral composition and rank of the

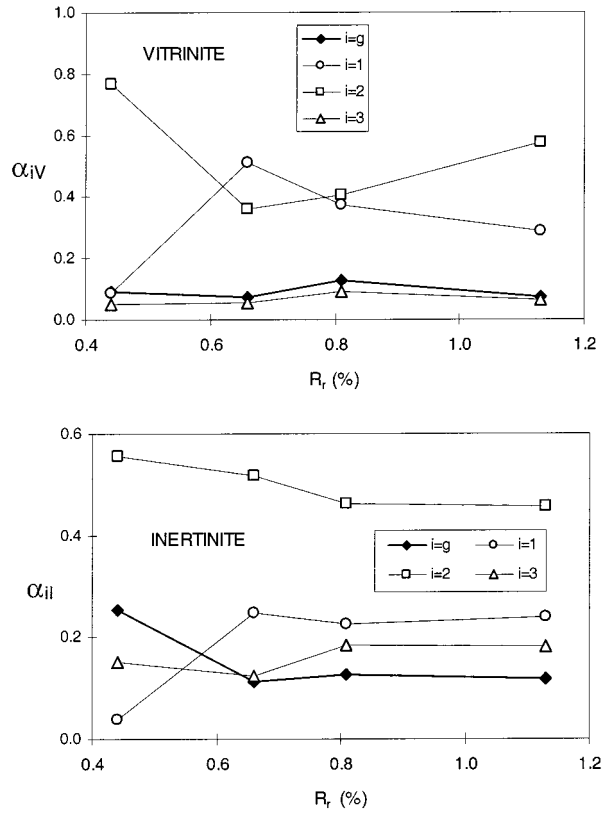

Figure 9. Variation of α_{iV} and α_{iI} with R_r.

samples, it must be first established the rank-dependent contributions of the different macerals to the total volatile matter release. This was carried out in a previous work of the authors,[11] in which a set of rank-dependent maceral functions $\phi_V(R_r)$, $\phi_L(R_r)$, and $\phi_I(R_r)$, representing the dry ash-free fraction of volatile matter in the pure maceral, were derived from a fitting procedure with data of more than 1000 coals in order to match the following equation:

$$\mathrm{VM} = \phi_V(R_r)X_V + \phi_L(R_r)X_L + \phi_I(R_r)X_I \qquad (7)$$

In this equation *VM* represents the calculated dry ash-free (daf) fraction of volatile matter in the coal, and X_V, X_L, and X_I are the volume fractions of vitrinite, liptinite, and inertinite in the mineral matter-free coal ($X_V + X_L + X_I = 1$). The analytical expressions and parameters of functions ϕ can be found in Borrego et al.[11] However, eq 7 can only be used if the predicted values are similar to those estimated from the TGA experiments. These can be calculated by the following expression:

$$\mathrm{VM_{TGA}} = \frac{(M_{30} - M_{900}) \times (f_g + \sum_{j=1}^{3} f_j)}{(M_{30} - M_{900}) \times (1 - f_a - f_b) + (M_{900} - M_f)} \qquad (8)$$

where M_{30} is the sample weight at the beginning of the heating ramp (30 °C), M_{900} is the sample weight at the end of the heating ramp under N_2 atmosphere (900 °C) and M_f is the sample weight after the combustion stage. It is assumed that only peaks *g*, *1*, *2*, and *3* contribute to the volatile matter release. Fractions f_a, f_b, f_g, and f_j are estimated by the deconvolution procedure using eq 3. Figure 3 shows a comparison between the values of volatile matter estimated from the TGA experiments (eq 8) and those calculated via eq 7 for all the samples indicated in Table 1. The average relative error was found to be $-3.0 \pm 7.7\%$, which falls within the confidence limits established by Borrego et al.[11] As expected, the values of $\mathrm{VM_{TGA}}$ are very similar to those evaluated by the UNE standard ($\mathrm{VM_{UNE}}$), with an average error as low as $2.7 \pm 5.1\%$ (Figure 3). Therefore, eq 7 can be used to obtain the normalized rank-dependent contributions of the different macerals to the total volatile matter release:

$$\Phi_V = \frac{\Phi_V X_V}{\mathrm{VM}} \quad \Phi_L = \frac{\Phi_L X_L}{\mathrm{VM}} \quad \Phi_I = \frac{\Phi_I X_I}{\mathrm{VM}} \qquad (9)$$

where $\Phi_V + \Phi_L + \Phi_I = 1$. To relate these maceral fractions to the DTG mass fractions of peaks *g*, *1*, *2*, and *3*, these must be also normalized as follows:

$$F_i = \frac{f_i}{f_g + \sum_{j=1}^{3} f_j} \quad i = g, 1, 2, 3 \qquad (10)$$

where therefore $F_g + F_1 + F_2 + F_3 = 1$. Assuming that there are neither synergetic nor antagonistic effects of the three maceral groups on the pyrolysis behavior, the following set of equations can be introduced:

$$F_i = \alpha_{iV}\Phi_V + \alpha_{iL}\Phi_L + \alpha_{iI}\Phi_I \quad i = g, 1, 2, 3 \qquad (11)$$

where parameters α_{iM} is the rank-dependent fractional apportioning of maceral *M* to peak *i* and $\alpha_{gM} + \alpha_{1M} + \alpha_{2M} + \alpha_{3M} = 1$ at any given rank. With these equations, the values of parameters α_{iM} at a given rank could be obtained if coals with values of Φ homogeneously distributed among the three macerals (i.e., three pure fractions of vitrinite, liptinite, and inertinite) were available at such a rank. This was not the case for the coals and fractions used in this work, in which liptinite was always present in a low amount ($X_L < 0.17$). To tackle this complication, the values of α_{iL} were assumed to be rank independent and were calculated from the DTG profile of a pure liptinite (KPB oil shale in Table 1). Figure 4 shows the results of the deconvolution procedure (open symbols = experimental points; continuous lines = individual peak profiles and calculated lumped reactivity) performed on the pyrolysis curve of KPB via eq 3. This experiment was performed at a heating rate of 25 °C/min, as were all the mentioned experiments thereinafter. According to eq 11 the values of α_{iL} for KPB are the same as those of fractions F_i ($\Phi_V = \Phi_I = 0$), which are indicated in Table 1. Therefore the rank-independent values of α_{iL} are $\alpha_{gL} = 0.08$, $\alpha_{1L} = 0.57$, $\alpha_{2L} = 0.30$, and $\alpha_{3L} = 0.04$. Since the amount of liptinite is quite low in all the studied coals and fractions, this assumption does not introduce an appreciable error in the calculations and permits the use of eq 11 in the following way:

$$F_i^c = F_i - \alpha_{iL}\Phi_L = \alpha_{iV}\Phi_V + \alpha_{iI}\Phi_I \quad i = g, 1, 2, 3 \qquad (12)$$

which, after the corresponding rearrangement, produces

$$\frac{F_i^c}{\Phi_V + \Phi_I} = \alpha_{iV} + (\alpha_{iI} - \alpha_{iV})\frac{\Phi_I}{\Phi_V + \Phi_I} \quad i = g, 1, 2, 3 \qquad (13)$$

Equation 13 can be used to obtain the values of α_{iV} and α_{iI} at different ranks, via a simple linear regression. This was done with the F_i^c values obtained for the hand-picked coals and density separated fractions (Table 1), for which two or three different values of $\Phi_I/(\Phi_V + \Phi_I)$ were available at fixed ranks ($R_r = 0.44$, 0.66, 0.81, and 1.13%). The regression plots are shown in Figures 5−8, together with the corresponding DTG profiles and model peaks from which the values of F_i^c were calculated. From the values of ordinate and slope obtained with the regression plots, the variation of α_{iV} and α_{iI} with rank was estimated (Figure 9). As mentioned above, these parameters represent the fractions of vitrinite (α_{iV}) and inertinite (α_{iI}) volatiles contributing to the different DTG peaks. Thus, Figure 9 clearly shows that the contribution of vitrinite to peaks *1* and *2* follows opposite trends with rank, with a maximum in peak *1*, and a corresponding minimum in peak *2*, for $R_r = 0.66\%$. On the other hand, the contribution of vitrinite to peaks *g* and *3* is nearly rank independent, with rank averaged values of 0.09 ± 0.03 and 0.07 ± 0.02 for α_{gV} and α_{3V}, respectively. Around half of the inertinite contribution to the total volatile matter release corresponds to peak *2* ($\langle\alpha_{2I}\rangle = 0.50 \pm 0.05$), slightly decreasing with rank. Inertinite contribution to peak *1* increases for low ranks and becomes stable ($\alpha_{1I} \approx 0.24$) for $R_r \geq 0.66\%$. The opposite applies for the contribution of inertinite to peak *g*, decreasing in the low rank range and reaching a stable value ($\alpha_{gI} \approx 0.12$) for $R_r \geq 0.66\%$. As happened with vitrinite, inertinite contribution to peak *3* is nearly independent of rank ($\langle\alpha_{3I}\rangle = 0.16 \pm 0.03$).

By interpolation of the data displayed in Figure 9, the values of α_{iV} and α_{iI} were estimated for all the coals indicated in Table 1. These values were used to calculate the corresponding fractions F_i, which were subsequently inputted as initial values in the deconvolution procedure of the DTG curves. Several examples of the analyzed DTG curves, corresponding to coals with values of random reflectance between 0.47 and 1.05%, are shown in Figure 10. The goodness of the resulting fittings can be clearly appreciated. The curve fittings for the rest of coals were similar and can be supplied on request. Coal VDR shows a peak at ∼720 °C (Figure 10) which corresponds to carbonates decomposition and therefore was not included in the deconvolution. This also happened with a few more samples (i.e., fraction DN8; Figure 7). After the deconvolution process, the values of fractions F_i (indicated in Table 1) hardly changed with respect to the initial values, as can be seen in the lower plot of Figure 10. This result implies that the trends depicted in Figure 9 by the continuous lines are true within the error inferred from Figure 10.

Finally, Figure 11 shows the variation with rank of the fractions F_i obtained with eq 11 for a hypothetical coal whose maceral composition were the average of those of the coals indicated in Table 1 ($\langle X_V\rangle = 0.69$, $\langle X_L\rangle = 0.06$, $\langle X_I\rangle = 0.25$). For this coal, peaks *g* and *3* would be nearly rank independent and each of them would amount for about 10% of the total pyrolysis yield. Peaks *1* and *2* would represent the highest part of the pyrolysis process (about 80% together), following opposite trends with rank, with a maximum in peak *1*, and a corresponding minimum in peak *2*, for $R_r = 0.66\%$. The area of peak *2* would be higher than that of peak *1* in all the studied range of reflectances, except for a narrow interval around 0.66%.

Trends of Kinetic Parameters. This section describes the relations obtained with maceral composition and coal rank of the Arrhenius parameters and temperatures of maximum peak reactivities evaluated from the deconvolution procedure. The analysis will be done on peaks *1*, *2*, and *3*, which are assumed to correspond to the primary and secondary pyrolysis processes of the model by Serio et al.,[4] since the temperature of maximum reactivity for peak *g* was always below 350 °C (average $Tm_g = 224$ °C). Besides, the average activation energy of peak *g* was 21000 ± 11000 J/mol (5.0 ± 2.6 kcal/mol), which is too low for a true chemical process. These facts permit us to speculate a relation between peak *g* and the process of desorption of guest molecules trapped in the coal matrix, as suggested before.

The kinetic parameters (activation energy, preexponential factor, and temperature of maximum reactivity) of peaks *1*, *2*, and *3* obtained for the different coals are indicated in Table 2. The highest values of activation energy correspond to peak *1* ($\langle E_1\rangle = 173000 \pm 30000$ J/mol) followed by peak *3* ($\langle E_3\rangle = 146000 \pm 15000$ J/mol) and peak *2* ($\langle E_2\rangle = 47000 \pm 8000$ J/mol). The temperatures of maximum peak reactivities are comprised in the following ranges: for peak *1* $Tm_1 = 416-475$ °C; for peak *2* $Tm_2 = 422-559$ °C, and for peak *3* $Tm_3 = 666-790$ °C. These ranges are similar to those corresponding to the three pyrolysis peaks reported by van Heek and Hodek[7] as indicated in former sections (peaks *1* and *2*: formation of tar and gases; peak *3*: decomposition of some oxygen-containing structures from the char with the formation of carbon monoxide and methane).

Figure 12 shows the existing relations between the preexponential factors and activation energies for the different peaks. The observed isokinetic effect for all the peaks can be expressed with an equation of the type

$$\ln(A_j) = a_j \times E_j + b_j \quad (j = 1, 2, 3) \qquad (14)$$

The values of parameters a_j and b_j for peaks *1*, *2*, and *3* are indicated in Figure 12. In general, the isokinetic effect can have two different origins. One is the existence of statistical autocorrelation between A_j and E_j[32] "if" the originating experimental data points (k_j) are true subsets of an universal set. The experimental subsets, which eventually produce the couples (A_j, E_j) in the isokinetic plot, must be understood as data sets of k_j values which are randomly distributed around the universal set within a given experimental error. On the other hand, the centers of gravity of the subsets, characterized by a given temperature T_o, must approximately coincide among them and with that of the true subset. This explanation of the isokinetic effect

(27) Mianowski, A.; Radko, T. Isokinetic effect in coal pyrolysis. *Fuel* **1993**, *72* (11), 1537−1539.

(28) Maki, T.; Takatsuno, A.; Miura, K. Analysis of pyrolysis reactions of various coals including Argonne Premium coals using a new distributed activation energy model. *Energy Fuels* **1997**, *11* (5), 972−977.

(29) Ungerer, P.; Pelet, R. Extrapolation of the kinetics of oil and gas formation from laboratory experiments to sedimentary basins. *Nature* **1987**, *327*, 52−54.

(30) Burnham, A. K.; Schmidt, B. J.; Braun, R. L. A test of the parallel reaction model using kinetic measurements on hydrous pyrolysis residues. *Org. Geochem.* **1995**, *23* (10), 931−939.

(31) de la Puente, G.; Marbán, G.; Fuente, E.; Pis, J. J. Modelling of volatile product evolution in coal pyrolysis. The role of aerial oxidation. *J. Anal. Appl. Pyrol.* **1998**, *45*, 75−87.

(32) Essenhigh, R. H.; Misra, M. K. Autocorrelations of kinetic parameters in coal and char reactions. *Energy Fuels* **1990**, *4*, 171−177.

(33) Boiko, E. A. Research on kinetics of the thermal processing of brown coals of various oxidative aging degree using the nonisothermal method. *Thermochim. Acta* **2000**, *348*, 97−104.

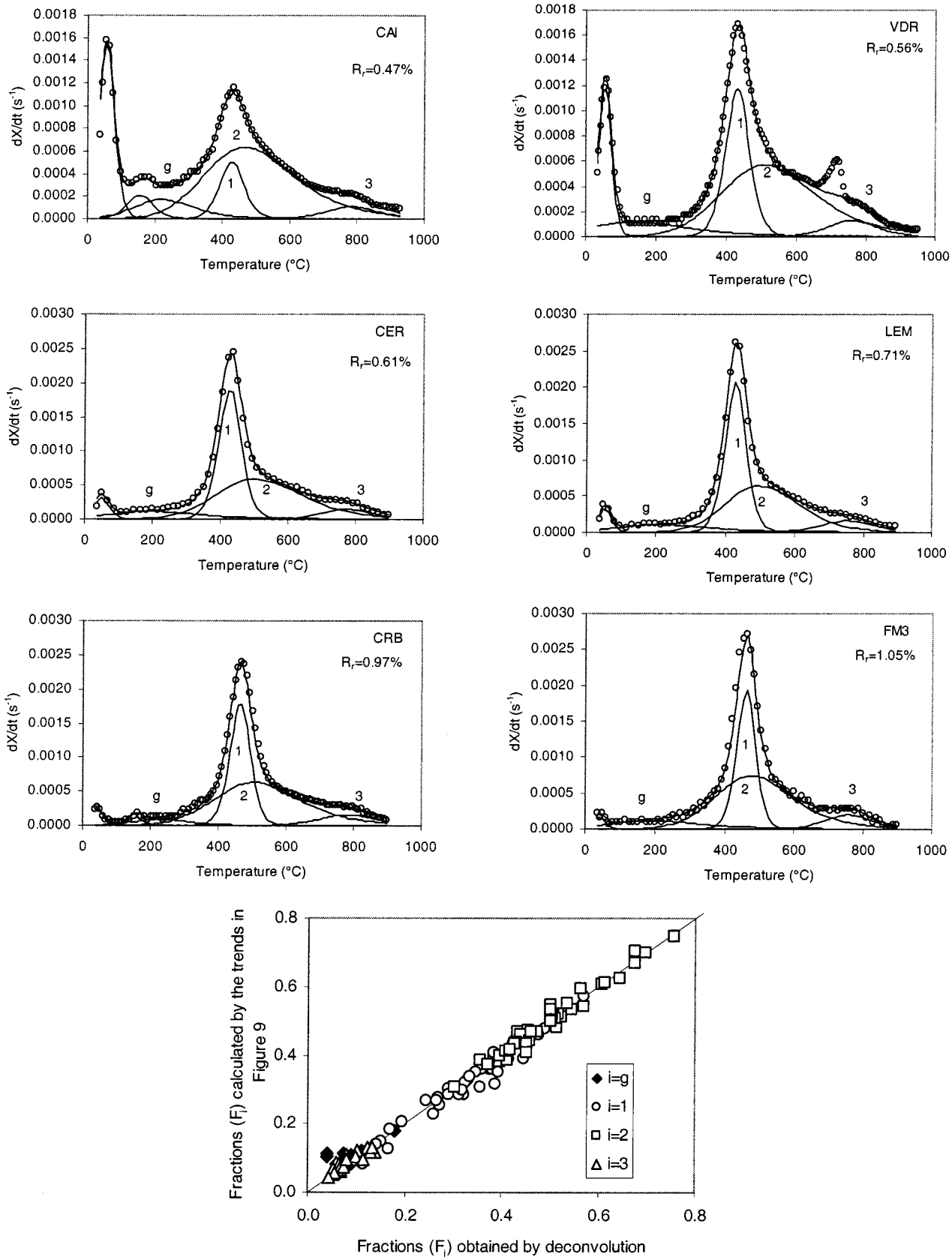

Figure 10. Examples of reactivity profiles and deconvolution results (β = 25 °C/min) for a number of coals with different ranks. Comparison between fractions F_i obtained by deconvolution and those calculated from the trends displayed in Figure 9.

must be clearly disregarded for the kinetic parameters obtained in this work, because the centers of gravity of the different data sets are rather different, as deduced from the values of Tm_j indicated in Table 2. In fact, the values of Tm_j, which correspond to ~50% peak conversion, can be taken as a good approximation for the values of T_o.

The other possible origin of the isokinetic effect is the *true* autocorrelation (not randomly based) of parameters A_j and E_j which provides fundamental (mechanistic)

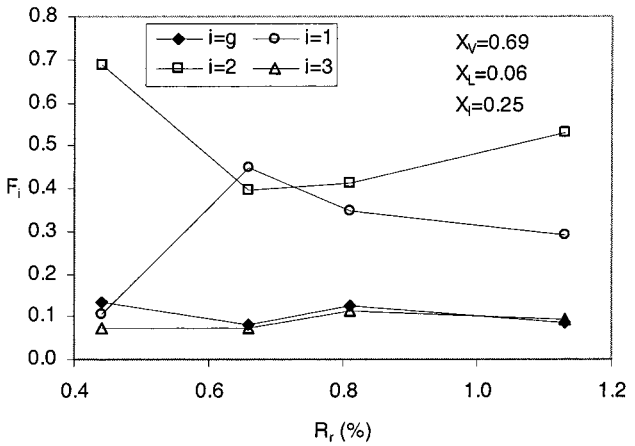

Figure 11. Variation of F_i with R_r for a model coal ($X_V = 0.69$, $X_L = 0.06$, and $X_I = 0.25$).

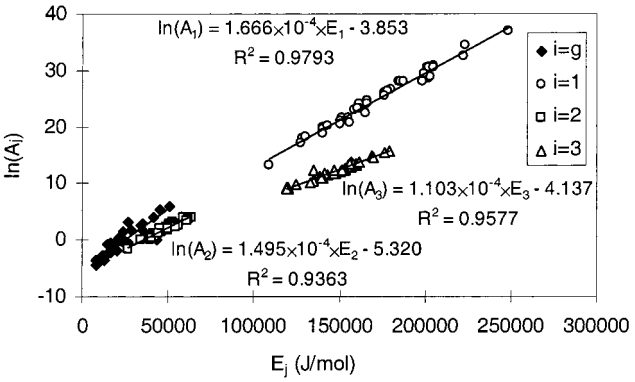

Figure 12. Isokinetic relations between E_i and A_i.

information on the relevant rate processes. This seems to be the case for the coal pyrolysis process. To gain insight into this mechanistic relationship of the kinetic parameters, both analytical and structural data of coals and chars would be required. This could be the object of future investigations.

One of the most common kinetic parameters used in the description of coal pyrolysis is the temperature of maximum global reactivity. This is almost coincident with the temperature of maximum reactivity of peak *1* (Tm_1), as can be appreciated in Figures 4 to 8 and 10, within the small deviations introduced by the overlapping of other peaks (mainly peak *2*). A specific parametric analysis was conducted on Tm_1 in order to relate this parameter to the coal type and rank. After testing a number of analytical expressions the following appeared to be the most suitable:

$$Tm_1 = Tm_1(R_r) + \Delta Tm_1(I_1) + \Delta Tm_1(L_1) \quad (15)$$

where $I_1 = \alpha_{1I} \cdot \Phi_I / F_1$ and $L_1 = \alpha_{1L} \cdot \Phi_L / F_1$ represent the normalized mass fractions of peak *1* that correspond to inertinite and liptinite, respectively. The parametric expressions of the different members of eq 15, as well as the values of the parameters obtained by using the algorithm Solver of Microsoft are indicated in Table 3. All members in eq 15 were found to be necessary for the minimization of errors. Thus, the average squared errors for different situations were found to be: (i) with all members in eq 15: 4.8×10^{-3}; (i) without $\Delta Tm_1(I_1)$: 6.8×10^{-3}; (iii) without $\Delta Tm_1(L_1)$: 5.5×10^{-3}; (iv) without $\Delta Tm_1(I_1)$, and without $\Delta Tm_1(L_1)$: 9.3×10^{-3}. Figure 13 permits us to visualize the dependences of Tm_1 with rank and maceral composition. It can be seen that there is an almost linear increase of Tm_1 with reflectance, from ~425 °C for $R_r \approx 0.4\%$ to ~480 °C for $R_r \approx 1.2\%$. This occurs in the absence of liptinite, whose presence produces a small diminution of Tm_1 of as much as ~6 °C. Inertinite has no effect on Tm_1 for $I_1 < 0.8$. For values of I_1 over ~0.8, a marked increase of Tm_1 can be appreciated. Figure 13 also offers a comparison between the values of Tm_1 obtained by the deconvolution procedure and those calculated by eq 15. A nice dispersion of points around the error zero line can be appreciated. The absolute error was found to be in all cases below 10 °C.

There is a high scattering of the activation energy of peak *1*, not shown in any figure but implied from Table 2, when plotted against coal type variables (V_1, I_1, and L_1) and rank (R_r). However, a clear correlation should arise from the fact that E_1 and A_1 are autocorrelated (isokinetic effect). Thus, combination of eqs 3, 4, and 14, and derivation of the resulting equation yields the following:

$$\frac{\beta E_j}{nR\, Tm_j^2 \exp\left[b_j - E_j \times \left(\frac{1}{R\, Tm_j} - a_j\right)\right]} = (1 - Xm_j)^{n-1} \quad (16)$$

In this equation β stands for the heating rate and Xm_j represents the conversion degree of peak j at the point of maximum reactivity. For peak *1*, this parameter is very similar for all coals, with an average value of 0.506 $\pm$ 0.011. As a result, eq 16 implies a correlation between E_1 and Tm_1 (E_1 increases with Tm_1) and therefore, according to the results shown in Table 3 and Figure 13, between E_1 and R_r, I_1 and L_1. In fact, by averaging the values of E_1 for the 30 coals indicated in Table 1, in groups of 5 coals of consecutive rank, a clear increase of $\langle E_1 \rangle_{5\ \text{coals}}$ with $\langle R_r \rangle_{5\ \text{coals}}$ can be appreciated (small graph in Figure 14). Yet the scattering of E_1 is very high, and can only be explained by the magnifying effect of eq 16 toward the local deviations from the isokinetic effect trend displayed in Figure 12. These deviations can be calculated for each peak by means of the following equation:

$$\Delta E_j = E_j \frac{\ln(A_j) - b_j}{a_j} \quad j = 1, 2, 3 \quad (17)$$

If ΔE_1 were simply a consequence of mathematical dispersion from the applied deconvolution procedure, one would expect to obtain a random distribution of values with any variable. However, when plotting ΔE_1 against Tm_1, a clear trend can be appreciated (Figure 14). A similar behavior was recently reported for kinetics of gasification of carbon materials[34] and the explanation which follows is derived from the conclusions reached there. It can be observed that the values of ΔE_1 grow almost linearly with Tm_1, with a difference between the lowest and the highest values of $\delta E_1 \approx$ 15000 J/mol. Since a_1 and b_1 were obtained by linear regression, the average value of ΔE_1 is obviously 0, and the distribution can be characterized by a standard deviation $\sigma_{\Delta E_1} = \pm 4400$ J/mol. With these results we

(34) Marbán, G.; Cuesta, A. On the cause of deviation of Arrhenius parameters form the isokinetic trend in carbon gasification reactions. *Energy Fuels*, submitted.

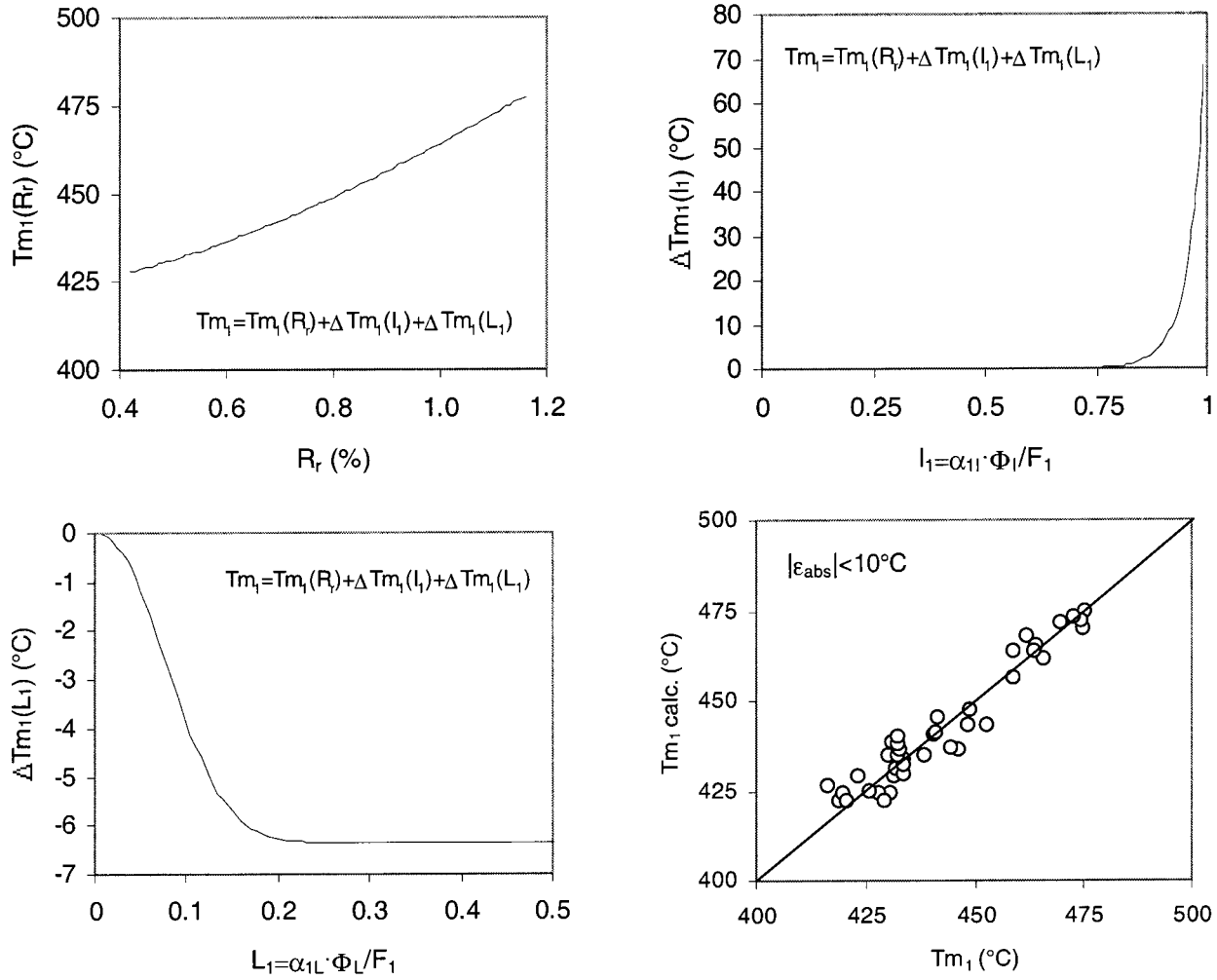

Figure 13. Calculated variations of the temperature of maximum reactivity for peak *1* as a function of rank (R_r), inertinite content (I_1) and liptinite content (L_1). Comparison between the experimental and calculated values of Tm_1.

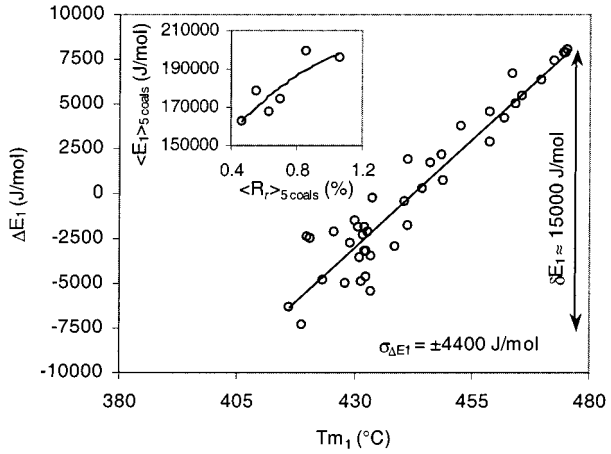

Figure 14. Variation of the discrepancies between the obtained activation energies and those expected from the isokinetic effect trend (ΔE_1) with the temperature of maximum reactivity for peak *1*. Small plot: variation of the averaged values of E_1, for groups of 5 coals of consecutive rank, with averaged random reflectance.

are tempted to believe that, in fact, ΔE_1 is related to the activation energy distribution within peak *1*. Thus as Tm_1 increases, the processes with higher activation energy within the small variation range of peak *1* are enhanced, according to the trend depicted in Figure 14. This fact is mathematically reproduced for a combination of three model peaks in the Appendix. In this sense, $\sigma_{\Delta E_1}$ can be interpreted as a characteristic parameter of the activation energy distribution of peak *1*. Then, it can be concluded that E_1 varies for the different coals according to two different causes: (i) its dependence with rank and maceral composition (in this case given by the variation of Tm_1 displayed in Figure 13 and the autocorrelation eq 16), which can affect greatly the energy value as observed in the small graph of Figure 14, and (ii) the distribution of processes, whose combination produces peak *1*, implies a narrow distribution of activation energies which results in a small increment of the activation energy with the increase of Tm_1 with respect to the activation energy expected from the isokinetic effect trend.

Finally, Figures 15 and 16 offer the obtained variations of activation energies with rank for peaks *2* and *3*, respectively. As observed in the lower plot of both figures, again the discrepancies between the obtained activation energies and those expected from the isokinetic effect trends (ΔE_2 and ΔE_3) are dependent on the temperature of maximum peak reactivity, although with a higher scattering than that observed for peak *1*. Thus, by applying the same arguments as for peak *1*, peaks *2* and *3* must also be formed by a combination of processes that produces a narrow distribution of activation energies ($\sigma_{\Delta E_2} = \pm 2000$ J/mol and $\sigma_{\Delta E_3} = \pm 3200$ J/mol). The values of E_2 and E_3 were found to be independent of

Table 2. Kinetic Results[a] Obtained from the Fitting of the DTG Curves ($\beta = 25$ °C/min)

code	R_r (%)	E_1 (J/mol)	E_2 (J/mol)	E_3 (J/mol)	ln(A_1)	ln(A_2)	ln(A_3)	Tm_1 (°C)	Tm_2 (°C)	Tm_3 (°C)
				Coals						
FG2	0.43	184203	34552	155442	28.1	0.0	13.1	419	443	762
FG3	0.46	161777	40962	156558	24.2	0.9	13.8	416	471	732
CAI	0.47	151220	39025	152255	21.7	0.6	12.3	431	471	786
CAS	0.48	128124	40367	157274	17.9	0.5	13.0	420	494	779
LEA	0.48	185552	41296	143059	27.9	1.2	11.6	428	458	761
FG1	0.49	140339	38537	145430	19.9	0.3	11.7	426	488	772
INS	0.55	200885	46119	159563	30.4	1.8	13.4	431	480	774
VDR	0.56	158508	42622	155059	22.9	0.8	13.1	432	508	760
GED	0.58	166488	48766	155009	24.7	2.2	13.0	423	488	764
DRA	0.59	223694	50595	141462	34.3	2.8	11.9	434	468	735
COS	0.60	205039	48632	138081	30.8	2.1	11.3	439	494	744
CER	0.61	160243	47695	152988	23.2	1.8	12.6	432	504	774
PT2	0.62	140128	55374	153486	19.5	2.7	12.3	434	531	790
BMC	0.64	187294	51649	134756	27.9	2.9	12.3	434	470	670
PT3	0.68	143211	63487	150670	20.3	3.8	12.2	430	552	780
SA1	0.68	180129	54685	136374	26.7	2.8	10.9	432	517	753
SA2	0.68	150664	55894	135180	21.0	2.6	10.5	446	548	769
LEM	0.71	176619	59094	134601	26.2	3.9	10.7	431	496	753
CRO	0.71	161322	61402	147682	23.4	3.6	11.8	433	541	782
KEL	0.73	202072	52499	120000	30.6	3.2	8.9	433	460	750
CAN	0.74	166434	49456	119372	23.9	2.2	9.2	441	494	730
BEN	0.76	177903	53415	134896	26.3	2.9	10.4	432	496	772
PHA	0.84	204693	38950	120104	30.5	0.6	9.1	442	469	738
CRB	0.97	199247	46068	133196	28.4	1.4	10.0	466	507	781
NOR	0.98	247933	46095	140122	37.0	1.9	11.0	459	474	775
BSE	1.03	150308	42692	160000	20.4	0.7	13.2	459	520	784
SBA	1.04	200393	43246	146357	28.7	1.3	11.8	464	478	775
FM3	1.05	222156	48652	169322	32.5	2.3	14.9	462	476	759
FM1	1.07	201934	49880	157478	28.5	1.8	13.3	475	537	764
HEI	1.14	202972	49910	179125	28.9	2.2	15.7	470	502	778
				Hand-Picked Coals						
M6	0.44	160164	26466	146951	23.3	−1.6	12.2	429	434	753
U26	0.44	130548	39842	156015	18.3	0.2	13.5	421	520	748
WA2	0.66	176534	53642	139681	25.5	2.5	11.1	445	524	767
BB2	0.66	127526	61338	151864	17.1	3.5	12.4	441	547	776
WWI	0.66	109076	54059	151762	13.2	2.2	12.5	464	559	774
				Density-Separated Fractions						
DN2	0.81	199677	45626	120362	29.3	1.9	9.2	449	459	732
DN5	0.81	154988	39427	124578	21.6	0.6	9.9	449	475	728
DN8	0.81	140359	40610	119258	18.9	0.3	9.0	453	521	738
VC2	1.13	198512	43390	176657	27.9	1.1	15.4	475	491	775
VC5	1.13	155797	44601	161179	20.8	1.3	13.7	474	498	766
VC8	1.13	165601	49739	170000	22.5	2.1	14.7	473	505	774

[a] R_r = random reflectance, E_i = activation energy of DTG peak i, ln(A_i) = natural logarithm of the preexponential factor (s^{-1}) of DTG peak i, Tm_i = temperature of maximum reactivity of DTG peak i.

Table 3. Results of the Parametric Analysis to Relate the Temperature of Maximum Reactivity of Peak *1* with Coal Rank and Type

members of equation: $Tm_1 = Tm_1(R_r) + \Delta Tm_1(I_1) + Tm_1(L_1)$		parametric expressions	parameter values
$Tm_1(R_r)$		$Tm_{1,0} + r_1R_r + r_2R_r^2 + r_3R_r^3$	$Tm_{1,0} = 423.393$ $r_1 = -19.039$ $r_2 = 78.942$ $r_3 = -19.269$
$\Delta Tm_1(I_1)$	$I_1 = \frac{\alpha_{1I}\Phi_I}{F_1}$	$i_1 \times (1 - (1 - I_1^{i_2})^{i_3})$	$i_1 = 448.967$ $i_2 = 19.699$ $i_3 = 0.096498$
$\Delta Tm_1(L_1)$	$L_1 = \frac{\alpha_{1L}\Phi_L}{F_1}$	$l_1 \times (1 - (1 - L_1^{l_2})^{l_3})$	$l_1 = -6.355$ $l_2 = 2.216$ $l_3 = 153.341$

maceral composition. On the other hand, there are clear trends of variation of E_2 and E_3 with rank, which are enclosed by the continuous lines depicted in the upper plots of Figures 15 and 16. It can be observed that the width of the activation energy intervals comprised by these lines is similar to the corresponding value of δE ($\delta E_2 \approx 9000$ J/mol and $\delta E_3 \approx 20000$ J/mol) estimated from the lower plots. In this sense, it can be concluded that the vertical variation of E_2 and E_3 in Figures 15 and 16, which might be mainly due to procedural errors, is also contributed by the narrow distribution of activation energies in peaks *2* and *3*, whereas the horizontal variation is a consequence of the rank variation. The latter involves a maximum in the activation energy of peak *2* for $R_r \approx 0.7\%$, and a minimum in the activation energy of peak *3* for $R_r \approx 0.8\%$. A more complete experimental procedure, including product analysis and char characterization, could help the understanding of these trends.

Conclusions

In this work, the global pyrolysis kinetics of a broad range of coals was studied by means of thermogravimetric experiments. An Arrhenius-based deconvolution model was applied to the obtained DTG curves in order to obtain reliable kinetic parameters for the different DTG peaks. The model assumes that the weight loss rate ascribed to volatile release during primary and secondary pyrolysis is a result of the parallel occurrence of three pseudo-unimolecular *n*th-order reactions (peaks *1*, *2*, and *3*). The kinetic results were expressed as a function of coal rank and maceral composition in order

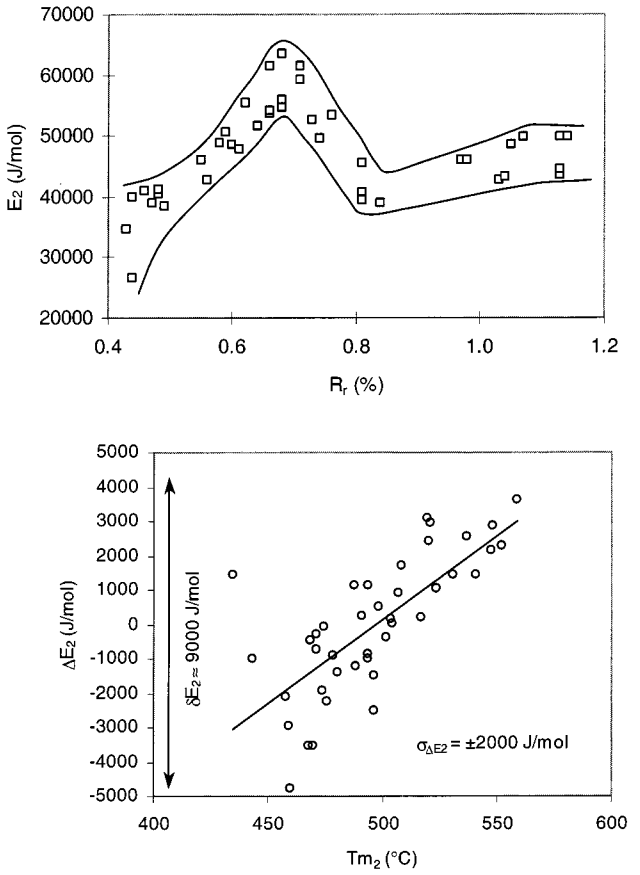

Figure 15. Variation of E_2 with random reflectance. Lower plot: variation of the discrepancies between the obtained activation energies and those expected from the isokinetic effect trend (ΔE_2) with the temperature of maximum reactivity for peak *2*.

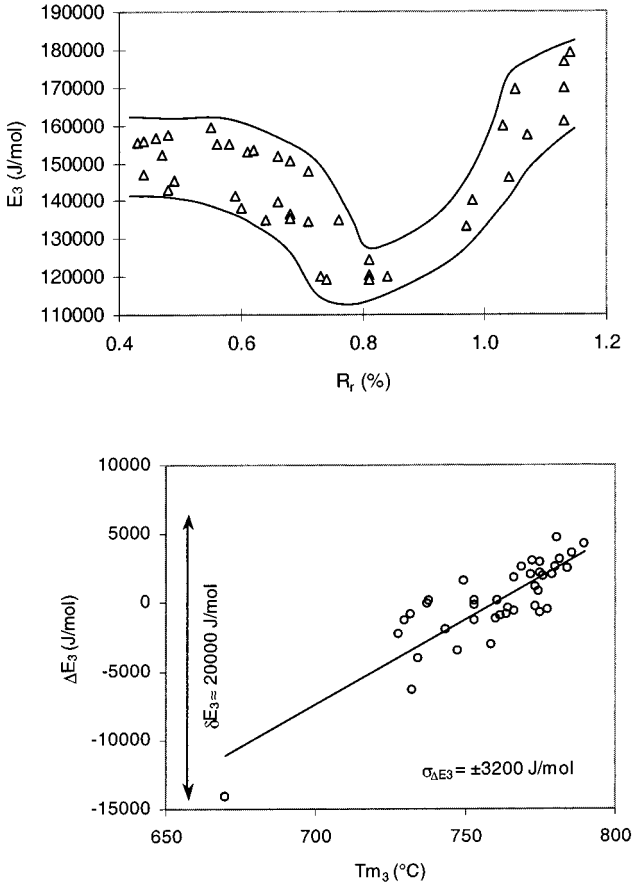

Figure 16. Variation of E_3 with random reflectance. Lower plot: variation of the discrepancies between the obtained activation energies and those expected from the isokinetic effect trend (ΔE_3) with the temperature of maximum reactivity for peak *3*.

to obtain reliable kinetic trends. From the work results, the following conclusions can be established:

• The average apparent reaction order was found to be 1.67.

• The mass fractions corresponding to peaks *1*, *2*, and *3* follow definite trends with rank ($0.43 \leq R_r \leq 1.14\%$) and maceral composition. The main part of volatile release (~80%) is ascribed to peaks *1* and *2*, whereas peak *3* accounts for about 10% of the pyrolysis yield.

• The temperature of maximum reactivity for peak *1* (Tm_1) is almost coincident with that of the maximum overall reactivity and follows clear trends with coal rank and type. A parametric analysis showed that this temperature increases with coal rank and slightly decreases with liptinite content. High values of inertinite content also provoke an increase on Tm_1.

• The activation energies of peaks *2* and *3* were found to be independent of coal type and related to coal rank.

• The kinetic parameters (activation energy and preexponential factor) of the three peaks exhibited clear isokinetic effects which are not caused by statistic correlations. The discrepancy between the values of activation energy calculated by the deconvolution procedure and those predicted by the isokinetic trends were found to be linearly dependent on the temperature of maximum reactivity for each peak. This relationship is ascribed to the existence of narrow distributions of activation energy within each peak.

Notation

a_j	Slope of the isokinetic relation between ln(Aj) and E_j ($j = 1, 2, 3$)
A_i	Preexponential factor of process i ($i = a, b, g, 1, 2, 3$), s^{-1}
b_j	Ordinate of the isokinetic relation between ln(Aj) and E_j ($j = 1, 2, 3$)
E_i	Activation energy of process i ($i = a, b, g, 1, 2, 3$), J/mol
f_i	Fraction of the total volatile release corresponding to process i ($i = a, b, g, 1, 2, 3$)
F_i	Normalized fraction of the total volatile release corresponding to process i ($i = g, 1, 2, 3$)
F_i^c	Normalized fraction of the total volatile release corresponding to process i ($i = g, 1, 2, 3$) after discounting the contribution of liptinite
I_1	Normalized mass fraction of peak *1* that corresponds to inertinite
k_i	Kinetic rate constant of process i ($i = a, b, g, 1, 2, 3$), s^{-1}
L_1	Normalized mass fraction of peak *1* that corresponds to liptinite
n	Apparent reaction order
R	Universal gas constant, J/(K mol)
R_r	Vitrinite random reflectance, %
t	Time, s
T	Absolute temperature, K
Tm_i	Temperature of maximum reactivity for process i ($i = g, 1, 2, 3$)
VM	Dry ash-free fraction of volatile matter in the coal calculated by eq 7

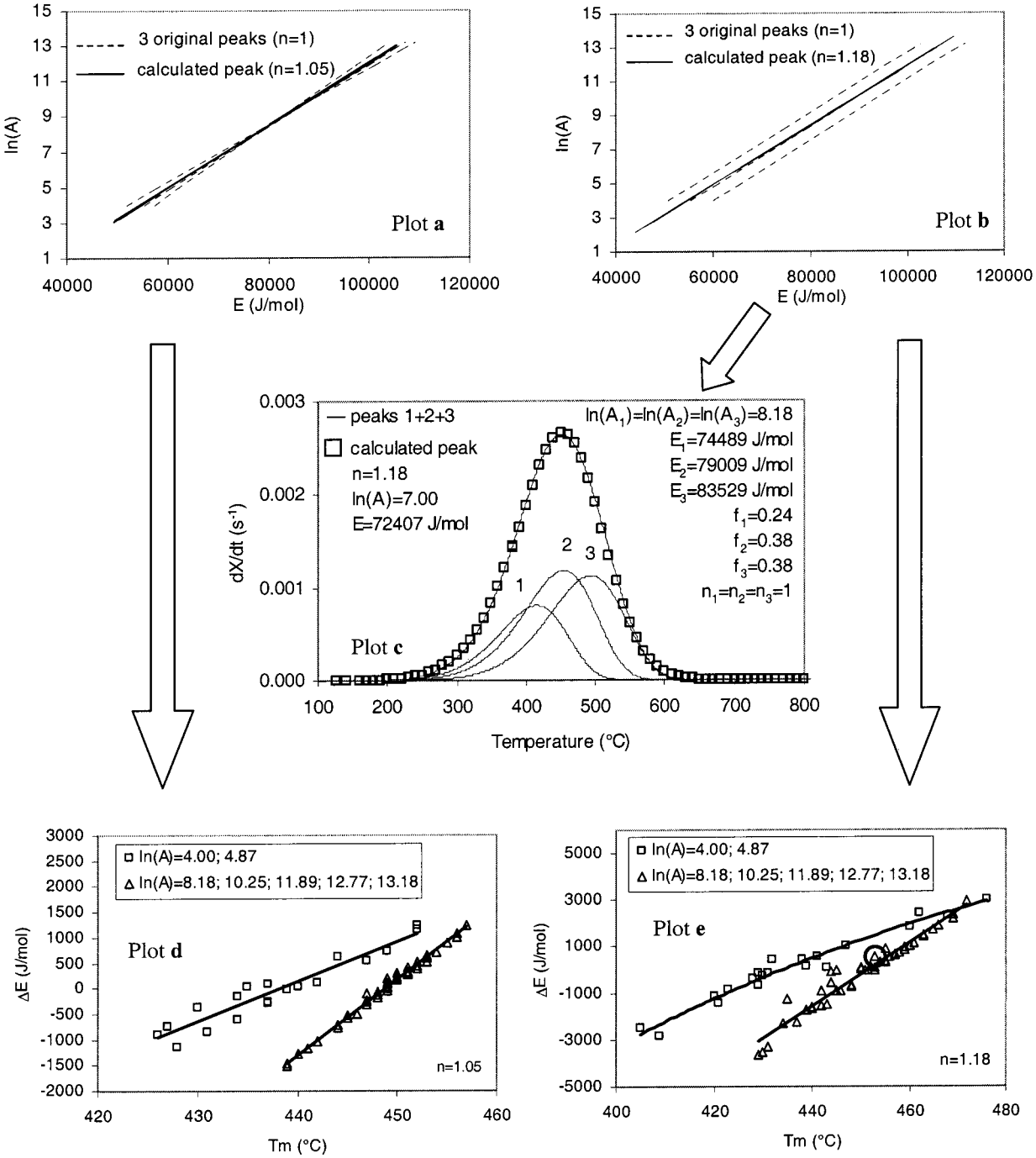

Figure 17. Plots: (a) Intersecting isokinetic trends of the originating peaks (dashed lines) and calculated isokinetic trend for the convolved peaks (solid line); (b) Parallel isokinetic trends of the originating peaks (dashed lines) and calculated isokinetic trend for the convolved peaks (solid line); (c) Example of three peaks distribution (common A and parallel isokinetic trends) and convolved peak; (d) Variation of ΔE with Tm for the convolved peaks obtained from the peak distribution with intersecting isokinetic trends; (e) Variation of ΔE with Tm for the convolved peaks obtained from the peak distribution with parallel isokinetic trends.

VM_{TGA}	Dry ash-free fraction of volatile matter in the coal calculated from TGA experiments
VM_{UNE}	Dry ash-free fraction of volatile matter in the coal calculated according to the UNE standard
X	Mass fraction of released volatiles at a time t
X_i	Mass fraction of released volatiles by process i (i = a, b, g, 1, 2, 3) at a time t
X_V	Volume fraction of vitrinite in the mineral matter-free coal
X_L	Volume fraction of liptinite in the mineral matter-free coal
X_I	Volume fraction of inertinite in the mineral matter-free coal

Greek Symbols

α_{iV}	Fraction of vitrinite in the volatile matter contributing to process i (i = g, 1, 2, 3)
α_{iL}	Fraction of liptinite in the volatile matter contributing to process i (i = g, 1, 2, 3)
α_{iI}	Fraction of inertinite in the volatile matter contributing to process i (i = g, 1, 2, 3)
β	Heating rate, K/s
ΔE_j	Deviation of the value of activation energy for process j (j = 1, 2, 3) from that estimated from the isokinetic trend

ϕ_V Rank-dependent dry ash-free fraction of volatile matter in pure vitrinite

ϕ_L Rank-dependent dry ash-free fraction of volatile matter in pure liptinite

ϕ_I Rank-dependent dry ash-free fraction of volatile matter in pure inertinite

Φ_V Fractional rank-dependent contribution of vitrinite to the volatile matter release

Φ_L Fractional rank-dependent contribution of liptinite to the volatile matter release

Φ_I Fractional rank-dependent contribution of inertinite to the volatile matter release

Acknowledgment. European financial support through project ECSC 7220/ED075 is gratefully acknowledged. The following colleagues are thanked for providing some of the coals and fractions used in this work: C. F. K. Diessel, W. Kalkreuth, M. Steller, L. Gurba, A. Depers. G. Marbán, and A. Borrego thank Consejo Superior de Investigaciones Científicas of Spain for the award of research contracts.

Appendix: Variation of the Discrepancy between the Calculated Activation Energy and That Expected from the Isokinetic Trend with the Temperature of Maximum Peak Reactivity

A model peak was formed by combination of three first-order peaks. An example of this can be seen in plot *c* of Figure 17. The preexponential factors of the originating peaks were identical, and their activation energies were calculated according to three corresponding isokinetic trends in two different situations. In a first situation the isokinetic trends were forced to intersect at a given point (dashed lines in plot *a* of Figure 17). In the second situation, the three isokinetic trends were parallel with each other (dashed lines in plot *b* of Figure 17). These trends were used to calculate the activation energies of the three first-order peaks plotted in Figure 17 (plot *c*) for a common $ln(A) = 8.18$ and random fractional areas (f_1, f_2, and f_3) indicated in the plot. The convolved curve was then fitted to a single Arrhenius peak (eq 3 for a single peak) in which the searched parameters were *A*, *E*, and *n*. This procedure was repeated for different sets of three peaks built by changing the preexponential factors (the natural logarithms of which are indicated in plots *d* and *e* of Figure 17) in both situations and by giving randomly selected values to their fractional areas. In a first stage, and average order *n* of the convolved peaks was calculated for both situations, resulting in 1.048 ± 0.004 for the intersecting isokinetic trends (plot *a* in Figure 17) and 1.182 ± 0.040 for the parallel isokinetic trends (plot *b* in Figure 17). This confirms the assumption that the apparent reaction order can be understood as a characteristic parameter of the activation energy distribution within each pyrolysis peak.

In a second stage the values of *n* were kept fixed, and only parameters *A* and *E* of the convolved peaks were calculated. *A* and *E* values ($n = 1.18$) for the convolved peak in plot *c* of Figure 17 (open squares) are indicated in the plot. The values obtained for other 70 different convolved peaks in each situation allowed the construction of the isokinetic trends depicted by the solid lines in plots *a* and *b* of Figure 17. It can be seen that these constitute a neat average of the isokinetic trends of the originating peaks (dashed lines). With the calculated trends, the values of ΔE for both situations were calculated and plotted versus the temperature of maximum reactivity of the convolved peaks. Plot *d* in Figure 17 displays the results obtained from the intersecting isokinetic trends and plot *e* for the parallel isokinetic trends. The point corresponding to the convolved curve in plot *c* (Figure 17) is enclosed in a circle in plot *e*. In both situations a clear increase of ΔE with *Tm* is observed, thus supporting the assessment that this increase for the pyrolysis peaks is caused by the distribution of activation energies within a single peak. A common feature of these plots is the existence of two converging trends for the points obtained from the convolved peaks with low/high values of preexponential factor. This could be the cause of the higher dispersion of the ΔE, *Tm* points for low values of *Tm* observed in Figures 14, 15, and 16.

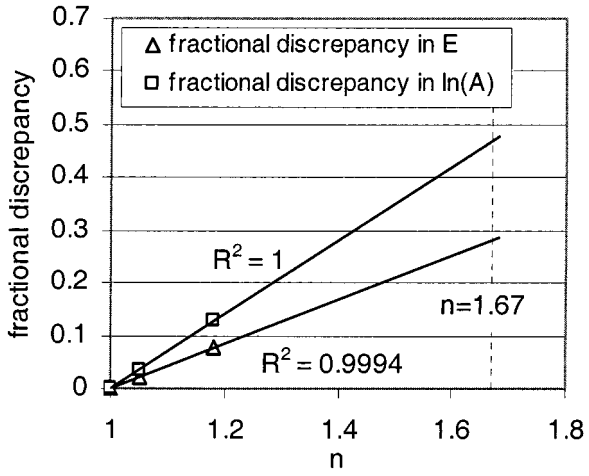

Figure 18. Variation with *n* of the discrepancy between the weighed averaged values of *E* and ln*(A)* for the originating first-order peaks and those calculated for the convolved peaks.

It was said that the estimated isokinetic trends (solid lines in plots *a* and *b* of Figure 17) constitute a neat average of the isokinetic trends of the originating peaks (dashed lines). However, the calculated values of *A* and *E* for the convolved peaks were in average lower than the weighed averaged values of the same parameters for the originating first-order peaks, which a priori seem to constitute a more realistic measure of the kinetic parameters for the convolved peak. This discrepancy must be considered when comparing kinetic parameters obtained for different reaction orders. Only as an example, Figure 18 shows the variation of the above-mentioned discrepancies for *E* and ln*(A)* (expressed as fractional relative deviations) with the value of apparent reaction order obtained for the situations displayed in Figure 17. The discrepancies seem to increase linearly with the reaction order. By interpolating the depicted trends for $n=1.67$ (reaction order used in this work) it would be realized that the values of activation energy obtained for the different DTG peaks were underestimated in average in more than 45% with respect to the weighed average values of activation energy derived from a hypothetical distribution of three first-order peaks that would be forming the DTG peaks. This, of course, should be further proved by obtaining trends for continuous distributions within each peak, and for higher reaction orders.

EF000170X